

Tetraspanin 33 (TSPAN33) regulates endocytosis and migration of human B lymphocytes by affecting the tension of the plasma membrane

Itze C. Navarro-Hernandez^{1,2} , Orestes López-Ortega³ , Ernesto Acevedo-Ochoa^{1,4} , Rodrigo Cervantes-Díaz^{1,5} , Sandra Romero-Ramírez^{1,5} , Víctor A. Sosa-Hernández^{1,3} , David E. Meza-Sánchez¹ , Guillermo Juárez-Vega¹, César A. Pérez-Martínez³, Bibiana Chávez-Munguía⁶, Arturo Galván-Hernández⁷ , Armando Antillón⁷, Iván Ortega-Blake⁷ , Leopoldo Santos-Argumedo³ , José M. Hernández-Hernández² and José L. Maravillas-Montero¹ 

1 Red de Apoyo a la Investigación, Universidad Nacional Autónoma de México e Instituto Nacional de Ciencias Médicas y Nutrición Salvador Zubirán, Mexico

2 Departamento de Biología Celular, Centro de Investigación y de Estudios Avanzados del Instituto Politécnico Nacional, Mexico City, Mexico

3 Departamento de Biomedicina Molecular, Centro de Investigación y de Estudios Avanzados del Instituto Politécnico Nacional, Mexico City, Mexico

4 Unidad de Investigación Médica en Inmunooquímica, Centro Médico Nacional Siglo XXI, Instituto Mexicano del Seguro Social, Mexico

5 Facultad De Medicina, Universidad Nacional Autónoma De México, Mexico

6 Departamento de Infectómica y Patogénesis Molecular, Centro de Investigación y de Estudios Avanzados del Instituto Politécnico Nacional, Mexico City, Mexico

7 Instituto de Ciencias Físicas, Universidad Nacional Autónoma de México, Cuernavaca, Mexico

Keywords

B lymphocyte; cytoskeleton; membrane tension; plasma membrane; tetraspanin

Correspondence

J. L. Maravillas-Montero, Red de Apoyo a la Investigación, Vasco de Quiroga No. 15, Belisario Domínguez Sección XVI, Tlalpan, Ciudad de México C.P. 14080, México
Tel: +52 (55) 5487 6080
E-mail: maravillas@cic.unam.mx

(Received 13 June 2019, revised 20 November 2019, accepted 16 January 2020)

doi:10.1111/febs.15216

B lymphocytes are a leukocyte subset capable of developing several functions apart from differentiating into antibody-secreting cells. These processes are triggered by external activation signals that induce changes in the plasma membrane properties, regulated by the formation of different lipid-bilayer subdomains that are associated with the underlying cytoskeleton through different linker molecules, thus allowing the functional specialization of regions within the membrane. Among these, there are tetraspanin-enriched domains. Tetraspanins constitute a superfamily of transmembrane proteins that establish lateral associations with other molecules, determining its activity and localization. In this study, we identified TSPAN33 as an active player during B-lymphocyte cytoskeleton and plasma membrane-related phenomena, including protrusion formation, adhesion, phagocytosis, and cell motility. By using an overexpression model of TSPAN33 in human Raji cells, we detected a specific distribution of this protein that includes membrane microvilli, the Golgi apparatus, and extracellular vesicles. Additionally, we identified diminished phagocytic ability and altered cell adhesion properties due to the aberrant expression of integrins. Accordingly, these cells presented an enhanced migratory phenotype, as shown by its augmented chemotaxis and invasion rates. When we evaluated the mechanic response of cells during fibronectin-induced

Abbreviations

AFM, atomic force microscopy; ECM, extracellular matrix; EGFP, enhanced green fluorescent protein; ERM, ezrin/radixin/moesin; EV, extracellular vesicles; gMFI, geometric mean fluorescence intensity; GSII, lectin II from *Griffonia simplicifolia*; MFI, mean fluorescence intensity; MMV, membrane-microvilli fraction; PFA, paraformaldehyde; PLL, poly-L-lysine; PNL, postnuclear lysate; RFP, red fluorescent protein; SEM, scanning electron microscopy; TEM, transmission electron microscopy; TEMs, tetraspanin-enriched domains; TSPAN33, tetraspanin 33; WGA, wheat germ agglutinin.

spreading, we found that TSPAN33 expression inhibited changes in roughness and membrane tension. Contrariwise, TSPAN33 knockdown cells displayed opposite phenotypes to those observed in the overexpression model. Altogether, our data indicate that TSPAN33 represents a regulatory element of the adhesion and migration of B lymphocytes, suggesting a novel implication of this tetraspanin in the control of the mechanical properties of their plasma membrane.

Introduction

Adhesion processes that allow cell attachment to surfaces, substrates, or other cells are recognized as essential for the morphogenetic development and maintenance of multicellular organisms [1]. The importance of adhesive properties is well established at the immune system, where they regulate relevant functions such as cell polarization, migration, and endocytosis [2–6].

Different subsets of leukocytes express diverse patterns of surface adhesion molecules that allow them to migrate and localize at specific anatomical sites to perform their functions [7]. Moreover, these patterns can be dynamically altered depending on the presence of several stimuli. The best-studied example occurs during inflammation when tissue damage or infection induces the recruitment of immune cells to the injury sites. During this process, leukocytes make dynamic transient contacts with different surfaces, all mediated by several adhesion molecules and their ligands [8,9]. Besides that, another crucial feature that governs the migration of leukocytes is their deformability potential that is controlled by changes in plasma membrane tension [10].

The membrane tension, defined as the force per length unit acting on a cross section of a cell membrane [11], is mainly modulated by the cytoskeleton. In the case of leukocytes, this is controlled through the active reorganization of the microfilaments that directly affect the formation of actin-dependent membrane protrusions such as microvilli, pseudopods, uropods, and the leading edge [10,12–19]. Previous studies have identified the role of membrane tension as a mechanical-triggered signaling mechanism essential for the activation and development of effector functions such as phagocytosis and cell polarization during migration [20,21]. For example, during immunological synapse formation between helper T and B cells or in a cytotoxic context, plasma membrane tension regulation is necessary for antigen discrimination and endocytosis, as well as for correct signal transduction by

the B-cell/T-cell receptors or activation of cytotoxic mechanisms [6,22,23]. These phenomena are accompanied and ultimately regulated by the clustering and recycling of a repertoire of surface signaling and adhesion molecules embedded in membrane microdomains such as lipid rafts and the tetraspanin-enriched microdomains (TEMs) [24]. These structures can regulate the spatiotemporal localization of molecules and control the deformability of membranes by altering the lipid and protein composition in specific regions of the lipid bilayer [25]. Microdomains also link the plasma membrane to the cortical actin cytoskeleton through intracellular molecules such as class I myosins, Rac/Rho GTPases, and ezrin/radixin/moesin (ERM) proteins, which, in turn, can control the polymerization of actin fibers and actin-dependent protrusions [26–29]. In sum, apart from the coordinated biochemical signals occurring during adhesive events, the coupling of mechanical signals, including regulation of membrane tension driven by modifications in the organization of membrane-associated molecules linked to the actin cytoskeleton, is necessary to perform diverse cellular functions.

As mentioned before, TEMs are among the membrane microdomains implicated in these phenomena. These plasma membrane structures have been involved in the compartmentalization of specific membrane components into multimolecular complexes [30]. The critical organizing elements of these aggregates are tetraspanins, a highly conserved family of small proteins with four transmembrane domains, two extracellular loops, and two short cytoplasmic domains [31]. These proteins are characterized by their ability to interact *in cis* with other molecules, establishing homo- or heterotypic associations with several partners, including transmembrane receptors, enzymes, adhesion molecules such as integrins, and signaling proteins [32].

The latest described member of the tetraspanin family is tetraspanin 33 (TSPAN33). This molecule, initially identified in mouse erythroblasts, exhibits a

restricted expression pattern that includes platelets, B cells, macrophages, and renal epithelial cells [33–37]. The native surface expression of this protein has shown to be inducible by different inflammatory activating stimuli in mammal cells. Furthermore, previous studies have suggested a role for TSPAN33 during Notch signaling, embryonic development, and in the immune response against multiple pathogens in invertebrates [35–40].

It has been reported that the absence of TSPAN33 in a murine model leads to splenomegaly, severe anemia, and, interestingly, a reduction of B-lymphocyte populations [34]. In 2013, it was reported that TSPAN33 is present and abundant in different Hodgkin and non-Hodgkin B-cell lymphoma samples from patients [35]. More recently, our group found that human primary B cells induce TSPAN33 protein expression after anti-CD40 and IL-4 stimulation and also, that is present at the early and late stages of human B-cell development [36].

Although we have established that TSPAN33 is expressed in different human B-cell subsets, its function(s) in these cells is not defined yet. Given the potential role of TSPAN33 at the plasma membrane of B cells, we explored in this work the implication of this tetraspanin in adhesion-controlled events such as phagocytosis/endocytosis, chemotaxis, and matrix invasion. We found that either overexpression or partial loss of TSPAN33 induces lymphocyte morphological alterations, defects in cell adhesion, and endocytosis that could be explained by the observed altered membrane tension.

Results

Overexpression of TSPAN33 promotes the formation of B-cell membrane protrusions

To assess the implication of TSPAN33 in B-cell function, we analyzed transgenic human Raji B cells, a stable control line expressing enhanced green fluorescent protein (EGFP) (Raji-EGFP), and another expressing a TSPAN33-EGFP fusion (Raji-TSPAN33). First of all, to corroborate this overexpression model, we measured TSPAN33 expression by western blot on both cell lines, finding that Raji-TSPAN33 cell shows a ~2.5-fold increase in the amount of TSPAN33 (considering both endogenous and EGFP-tagged fusion protein) when compared to control cells (Fig. 1A).

One singular attribute that we noticed once Raji-TSPAN33 cells were observed by fluorescence confocal microscopy was the effortlessly detectable microvilli

over the cell surface, longer and more abundant than the corresponding structures present over the control cells (Fig. 1B). To confirm these observations, we analyzed the cells with transmission electron microscopy (TEM), founding the same microvilli enhancement with longer and more abundant protrusions (Fig. 1C).

Since TSPAN33-EGFP seems to be localized at these actin-dependent structures, we performed a microvilli isolation procedure, capable of separating them from the rest of the cell body; in this way, we were able to detect an enrichment of TSPAN33 in microvilli fractions when compared to the cell body fraction using western blot (Fig. 1D). Here, we also detected actin and ezrin to serve as positive controls as they are molecules that can be found preferentially located at B-cell microvilli. Conversely, the detection of tubulin and nucleoporin as molecules that should be excluded from microvilli fraction validates our observations [41]. Additionally, we also observed that TSPAN33-EGFP preferentially localizes microvilli by probing these structures through LifeAct peptide-red fluorescent protein (RFP) transient expression, demonstrating the colocalization of microfilaments and TSPAN33-EGFP in live cells (Fig. 1E).

The emission of membrane protrusions is a crucial step in cell adhesion and migration of leukocytes. Since microvilli structures were extremely evident when Raji cells overexpressed TSPAN33, we hypothesize that other membrane-dependent projections could also be affected by this protein; therefore, we carried out assays to induce the spreading response developed by Raji-EGFP and Raji-TSPAN33 cell lines, when they were placed over fibronectin and stained for actin filaments [as previously described in Ref. [42] (Fig. 1F, left pictures)]. Although Raji-TSPAN33 cells did not show significant differences in the spreading area that they reached when compared to the Raji-EGFP control cells or in the number of protrusions, they were observed polarized, as its higher length/width coefficient confirmed it. Values closer to 1.0 indicate a more rounded morphology; elongation of the cells then corresponds to factor values > 1.0 and increases proportionally as the length of the cell increases (Fig. 1F, right panels). Additionally, we observed that these membrane extensions were longer and thicker in Raji-TSPAN33 cells (Fig. 1F, lower right panels).

TSPAN33 is present in vesicular structures of B cells

Beyond its expected plasma membrane typical residence, our micrographs also showed TSPAN33-

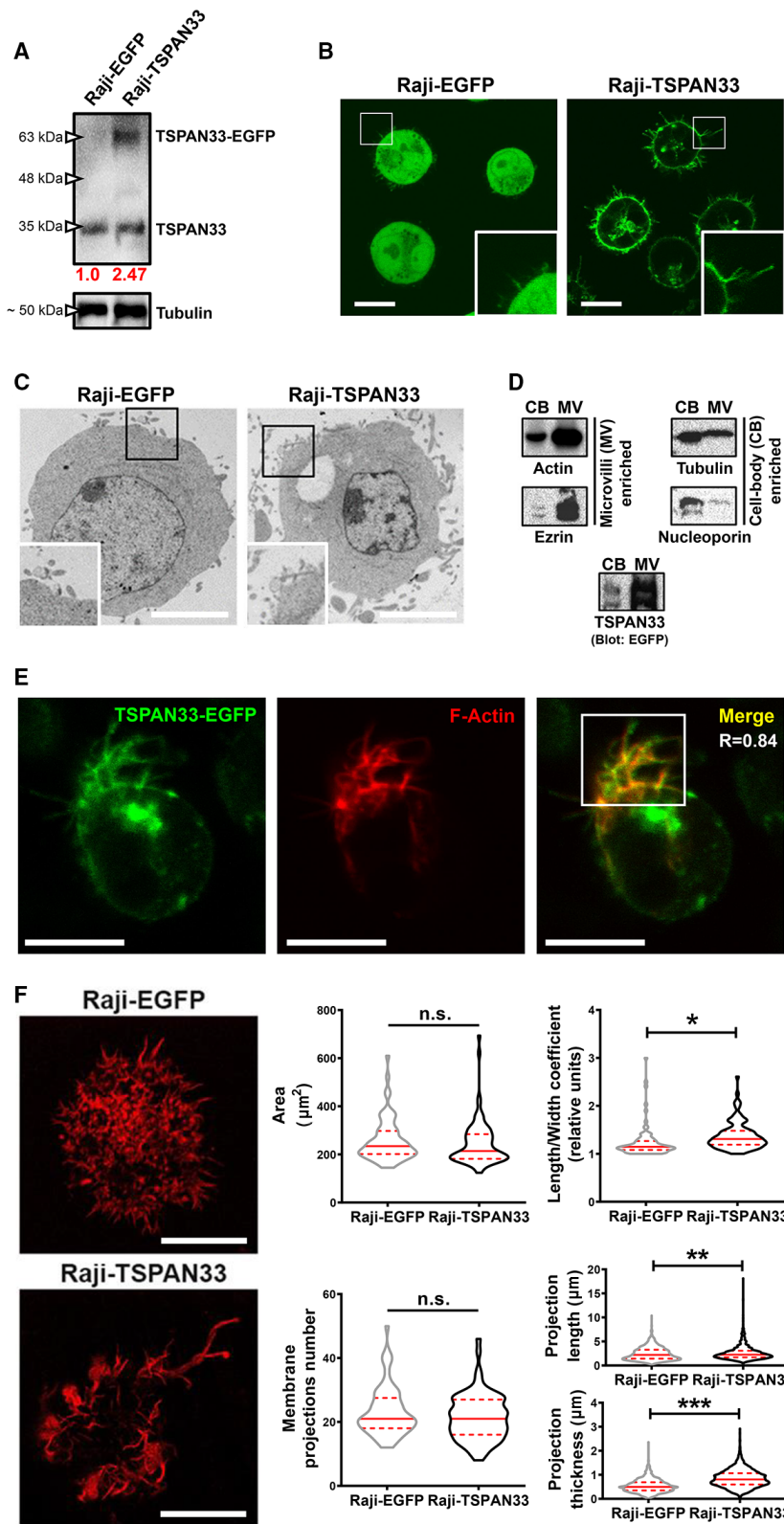


Fig. 1. TSPAN33 promotes plasma membrane/cytoskeleton-dependent B-cell protrusions. (A) Western blot analysis from Raji-EGFP and Raji-TSPAN33 was performed to detect endogenous (untagged) TSPAN33 and TSPAN33-EGFP fusion protein. Tubulin was used as the loading control. The red numbers show the fold difference in expression of TSPAN33 (including both endogenous and tagged forms in the case of Raji-TSPAN33 sample), once lanes were normalized against loading control as indicated in the Materials and methods section. The experiment shown is representative of three performed. (B) Confocal images of live Raji-TSPAN33 or Raji-EGFP cells in basal conditions; in these images, we appreciate membrane microvilli, more evident in Raji-TSPAN33 cells. Representative images of eight independent observations (10 fields each) per cell line are displayed. The bars represent 10 µm. (C) Microvilli structure and morphology as seen by TEM in Raji-EGFP and Raji-TSPAN33 cells. Representative pictures of a total of 20 individual cells captured (of each cell line) are presented. The bars represent 5 µm. (D) Microvilli enrichment in Raji cells assessed by the shear-based procedure described in Materials and methods. Equal amounts (40 µg) of total protein of MMV and the PNL were analyzed with WB for the detection of TSPAN33, actin, tubulin, nucleoporin, and ezrin. The blots shown are representative of three independently performed experiments. (E) Images of live Raji-TSPAN33 cells transiently transfected with pLifeAct; in these images, we appreciate the localization of the EGFP and F-actin-RFP and the colocalization of these denoted as Pearson's correlation coefficient (R). Representative micrographs of a total of 20 cells captured are shown. The bars represent 10 µm. (F) Raji-TSPAN33 or Raji-EGFP cells were placed over fibronectin-covered coverslips for 2 h; then, these cells were fixed and stained with TRITC-phalloidin to finally be analyzed by confocal microscopy. The bars represent 10 µm. Graphs show several parameters obtained from the analysis of these spread cells: area or length/width coefficient and number, length, and thickness of membrane projections. The values were derived from three independent experiments, measuring 100 cells in each one. Values are displayed as mean (solid red line) plus lower and upper quartiles (dotted red lines). The data were analyzed by an unpaired two-tailed Student's *t*-test. ****P* ≤ 0.001, ***P* ≤ 0.005, **P* ≤ 0.01.

EGFP localized at internal compartments of Raji cells; we found an enrichment of this tetraspanin at small cytoplasmic vesicles (Fig. 2A) and, more evidently, at bigger membranous organelle aggregates. By using wheat germ agglutinin (WGA) and lectin II from *Griffonia simplicifolia* (GSII), we could colocalize TSPAN33-EGFP at the Golgi apparatus, particularly at the trans-Golgi network (Fig. 2B).

Besides TSPAN33 presence at intracellular compartments, when the fibronectin-induced spread cells were analyzed by scanning electron microscopy (SEM), we observed an unusual finding. Numerous structures in the form of vesicles seem to be originated from the membrane extensions (Fig. 2C, left panels) that were much more abundant in Raji-TSPAN33 than in Raji-EGFP cells; accordingly, these cells upregulated the production of these vesicles by ~2-fold (Fig. 2C, right panel). Guided by this observation, we performed an extracellular vesicle enrichment by precipitation of Raji-TSPAN33 and Raji-EGFP cell culture supernatants followed by ultracentrifugation procedures. The resulting preparations were observed by TEM to found abundant vesicles below ~150 nm in diameter in both cell types; interestingly, the TSPAN33 transgenic cells seemed to generate more heterogeneous and bigger-sized vesicles (Fig. 2D). Furthermore, when these fractions were subjected to SDS/PAGE, we distinguished the presence of TSPAN33-EGFP fusion (but not EGFP alone) detected through EGFP blotting, thus demonstrating that TSPAN33 is recruited to these extracellular vesicles (EV) (Fig. 2E).

TSPAN33 plays a role in B-cell adhesion and migration

Once that we found that TSPAN33 expression levels could alter the morphological phenotype of our cells, we decided to evaluate other membrane and underlying cytoskeleton-related functions such as adhesion and migration. First, we performed cell adhesion assays using fibronectin and laminin as substrates. As depicted in Fig. 3A, Raji-TSPAN33 cells showed significantly reduced attachment to fibronectin and lesser extent laminin, when compared with control cells. According to previously generated data from our group [41,43], reduced cell adhesion capacity in B cells is usually accompanied by a defect in adhesion molecule surface expression, predominantly, integrins. Consequently, we decided to quantify the expression levels of these proteins on the plasma membrane by flow cytometry. As expected, we found significantly impaired expression of β1 (CD29) and β2 (CD18) integrins in the plasma membrane of Raji-TSPAN33 (Fig. 3B).

As Raji-TSPAN33 cells were less adherent and exhibited a decreased β1/β2 integrin surface expression, a phenotype that could be associated with defective cell migration [41,43], we proceeded to evaluate their chemotactic response. Since Raji cells were previously reported to respond and migrate to CCL21 gradients, through its receptor CCR7 [44], we used this chemokine to induce the motility of our transgenic Raji B cells. We determined that Raji-TSPAN33 cells exhibit significant differences in their chemotactic rates, as depicted by their increased

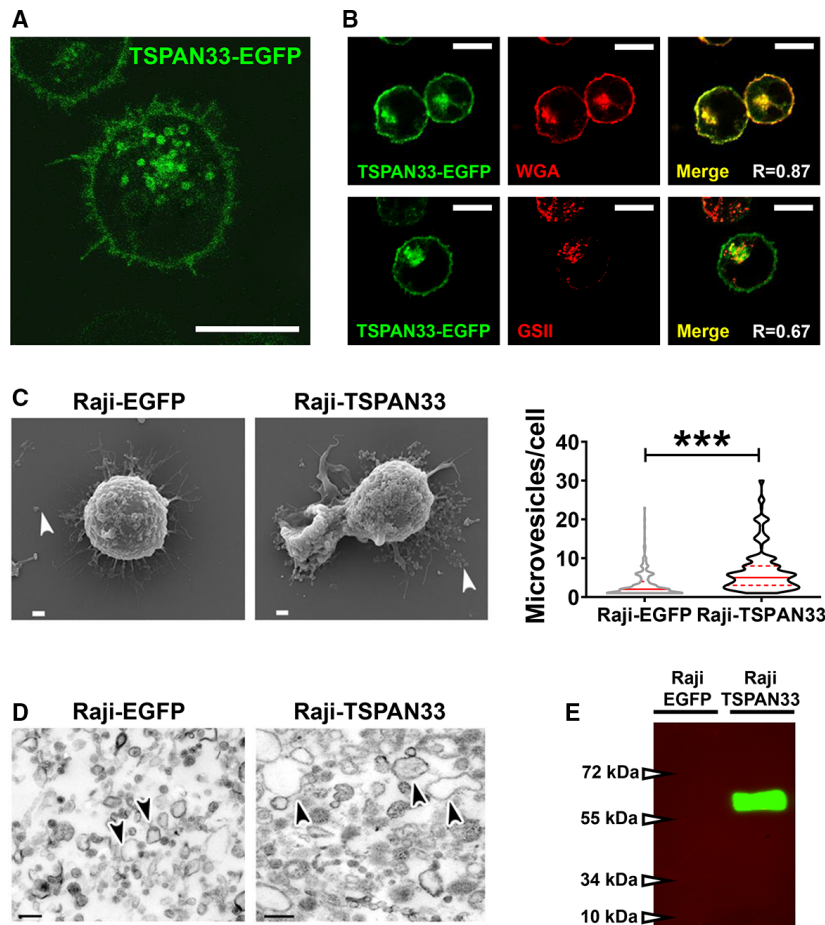


Fig. 2. TSPAN33 is present in vesicular compartments and EV of B cells. (A) Live Raji-TSPAN33 cell in basal conditions with the presence of TSPAN33 in vesicular compartments. A representative picture of eight independent observations (10 fields each) is displayed. The bar represents 10 μ m. (B) Raji-TSPAN33 cells were stained with WGA and GSII lectins to show the localization of TSPAN33 in the membrane/Golgi apparatus and the trans-Golgi network, respectively. Representative image of three independent stains performed (observing five fields each). R = Pearson's correlation (colocalization) coefficient. Bars represent 10 μ m. (C) Raji cells were placed on fibronectin-covered coverslips for 2 h; these cells were fixed and then were processed for SEM. The arrows show the presence of microvesicles. The bars represent 1 μ m. The graph shows the number of microvesicles in these cells, originated from the analysis of a total of 50 cells from at least three independent experiments, displayed as mean (solid red line) plus lower and upper quartiles (dotted red lines). These data were analyzed by an unpaired two-tailed Student's t -test. *** $P \leq 0.001$. (D) TEM of the microvesicles enriched by PEG8000 precipitation. Arrows depicted the different EV obtained. The bar represents 1 μ m. (E) Western blot of the enriched fraction of EV, showing the presence of TSPAN33-EGFP. The blot shown is representative of three independently performed experiments.

Euclidean migration distance values (which represents the shortest distance between cell paths start and endpoints) and their higher directionality values (that correlates with a more straight path that they follow in the gradient of the chemokine), even though there were no significant differences in other kinetic parameters such as accumulated migration distance or their absolute velocity (Fig. 3C). Considering these results and working with lymphoma Raji cells that were previously reported to present an aggressive invasive phenotype [45], we decided to

perform a transwell invasion assay in Matrigel (Fig. 3D, left panel). By this approach, we were able to assess that Raji-TSPAN33 cells were more invasive than control cells, either with or without CCL21 chemotactic stimulation (Fig. 3D, right panel). Finally, to prove that migratory and invasiveness differences observed between our cell lines were not due to variations in CCR7 expression, we measured it by flow cytometry and found no significant differences in TSPAN33-overexpressing and control cells (Fig. 3E).

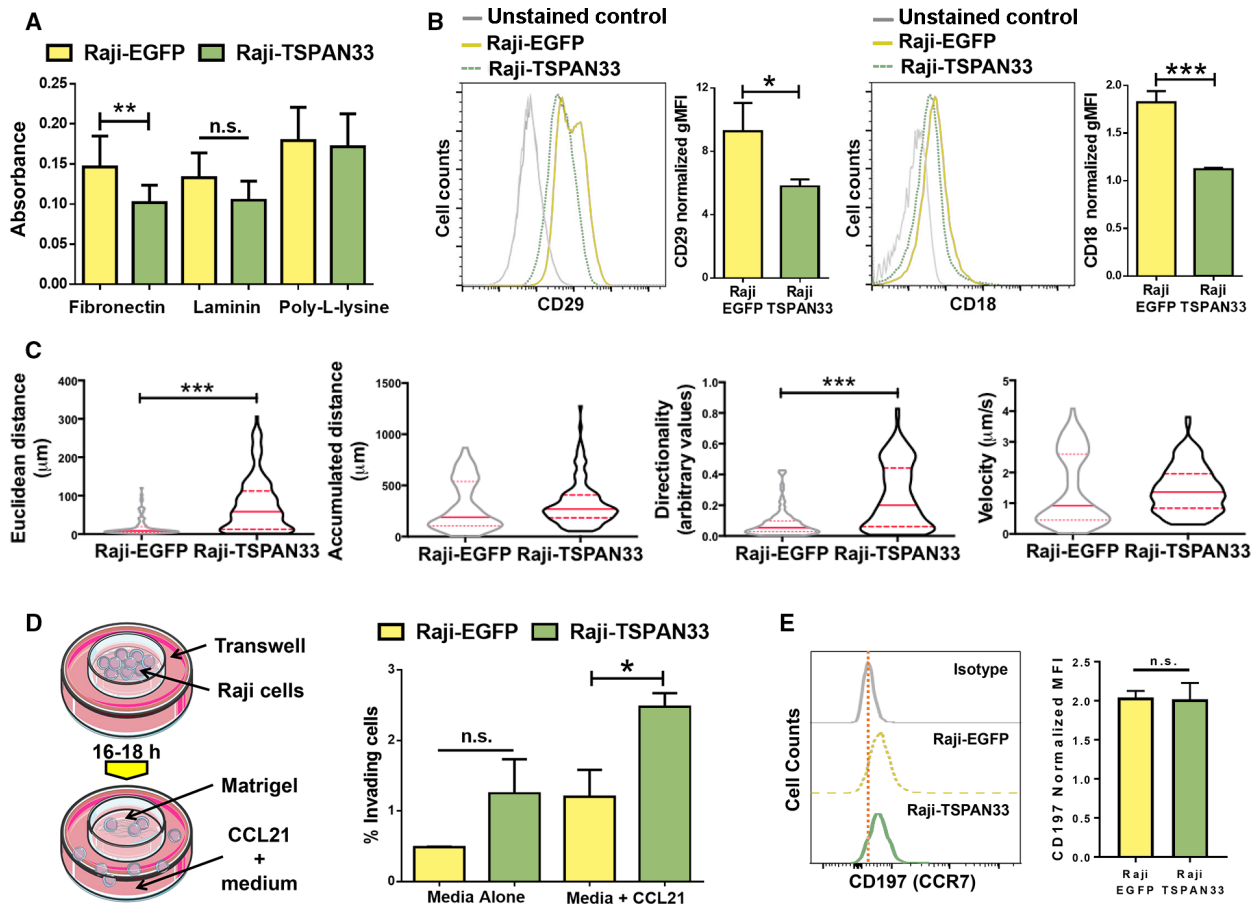


Fig. 3. TSPAN33 in Raji cells participates in adhesion and migration. (A) Equal numbers of Raji cells were placed on PLL, fibronectin, or laminin-covered coverslips for 30 min, after that the cells were fixed and stained with crystal violet. The absorbance of each sample was determined and plotted from data of four independent experiments. Values are displayed as mean \pm SD. The data were analyzed by an ANOVA with Bonferroni's post hoc test. **P \leq 0.005. (B) Histograms showing the expression of CD29 and CD18 in Raji-EGFP (solid yellow histograms) and Raji-TSPAN33 (dashed green histograms) cell lines, stained, and analyzed by flow cytometry. The gray histograms correspond to unstained cells' negative controls. The accompanier bar graph is derived from three independent tests; the normalized gMFI \pm SD is shown. These data were analyzed by an unpaired two-tailed Student's t-test. ***P \leq 0.001, *P \leq 0.05. (C) Raji cells of both groups were placed over fibronectin-covered coverslips for 30 min; after that period, the coverslips were mounted in a Zigmond chamber to allow the cells to be exposed to a gradient of CCL21 and capture their migratory paths using a confocal microscope. The graphs show the Euclidean and accumulated distance, directionality, and velocity of these migratory cells. The values were originated from four independent experiments. Data are presented as mean (solid red line) plus lower and upper quartiles (dotted red lines) and were analyzed by an unpaired two-tailed Student's t-test. ***P \leq 0.001. (D) Raji cells were placed in transwell upper chambers, previously covered with Matrigel; the cells were then exposed to a gradient of CCL21 or just medium, for 16–18 h. The migrated cells in the lower chamber were counted by flow cytometry. The graph shows the percentage of invading (migrated) cells regarding total cells. The values were derived from three independent experiments. Data are presented as mean \pm SD and were analyzed by an ANOVA with Bonferroni's post hoc test. *P \leq 0.05. (E) Histograms showing expression of CCR7 (CD197) in Raji-EGFP and Raji-TSPAN33 cell lines. The accompanier bar graph is derived from three independent tests; the normalized MFI \pm SD is shown. These data were analyzed by an unpaired two-tailed Student's t-test.

TSPAN33 regulates phagocytosis in B cells

As cell motility and adhesive properties seem to be affected by TSPAN33, we proceeded to evaluate the phagocytosis ability of these leukocytes, since this property is a vital component of immunity shared by TSPAN33-expressing human leukocytes, such as B cells and macrophages [37,46–51]. We started by

measuring the Raji cell uptake of fluorescent *Escherichia coli* bacteria expressing RFP. When our cell lines were observed by confocal microscopy, we could easily detect bacteria attached to the surface or internalized in most of the control cells, but not in Raji-TSPAN33 cells (Fig. 4A). This observation was corroborated using flow cytometry at single-cell level, finding a significant deficit on the attachment/

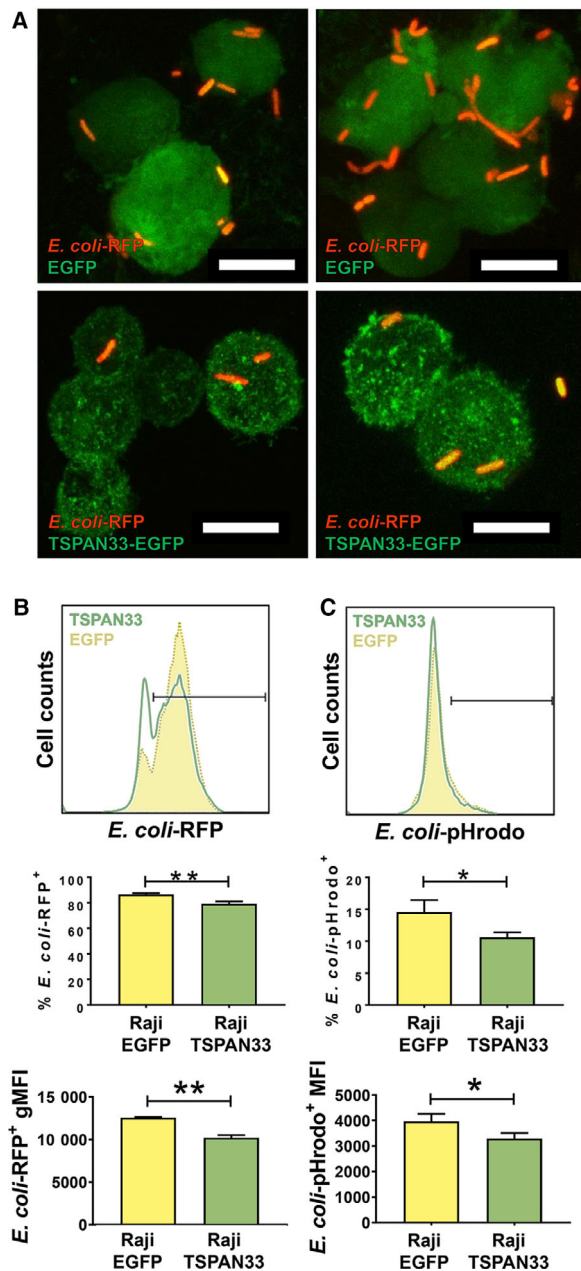


Fig. 4. TSPAN33 alters the phagocytosis of bacteria in B cells. Raji cells stably expressing TSPAN33-EGFP or EGFP were incubated at 37 °C for 3 h in the presence of live *E. coli*-RFP (A, B) or pHrodo *E. coli* bioparticles (C), then fixed, and analyzed by confocal microscopy or flow cytometry. The pictures shown are representative of four experiments performed. Bars represent 10 µm. For the fluorescence intensity analyses, the gMFI of bimodal data distributions were considered while the arithmetical MFIs were obtained for Gaussian data distributions. Histograms show a representative experiment with three replicates. Graphs present percentages of positive cells or MFI values ± SD. Data were analyzed by an unpaired two-tailed Student's *t*-test. ***P* ≤ 0.005, **P* ≤ 0.05.

phagocytosis rate in the Raji-TSPAN33 cells measured as percentage of *E. coli*-RFP⁺ cells (Fig. 4B, upper panels) and determining the geometric mean fluorescence intensity (gMFI) of this population (Fig. 4B, lower panel). *E. coli* marked with pHrodo-Red (*E. coli*-pHrodo) were used to discriminate surface-attached from phagocytosed bacteria. As this fluorogenic dye increases its fluorescence when pH becomes more acidic, the signal detected from this fluorochrome can be related to effectively phagocytosed particles. Using this approach, we confirmed the mentioned defect in the Raji-TSPAN33 cells denoted as a consistent lower percentage of *E. coli*-pHrodo⁺ cells (Fig. 4C, upper panels) and a significant lower pHrodo⁺ cell mean fluorescence intensity (MFI), when compared with the control cells (Fig. 4C, lower panel).

TSPAN33 modifies B-cell membrane mechano-response

Since the expression of TSPAN33 impaired the adhesive properties and altered the plasma membrane morphology of our transgenic B cells, we hypothesized that this tetraspanin could be regulating the plasma membrane tension through modifications in cell membrane deformability.

A feature that reflects the physiological status of cells is plasma membrane roughness [52,53]. By using atomic force microscopy (AFM), we were able of reconstructing the membrane topography of both Raji-EGFP and Raji-TSPAN33 adhered cells (Fig. 5A), observing that initial roughness of control cells over poly-L-lysine (PLL) is significantly reduced when they are exposed to fibronectin, since they undergo spreading processes accompanied by the flattening of their membrane. Strikingly, this effect was completely absent in Raji-TSPAN33 cells (Fig. 5B).

Since membrane flattening is a normal consequence of cell spreading, but we cannot detect it in our Raji-TSPAN33 cells, we measured changes in their plasma membrane stiffness. In these experiments, we analyzed the characteristics of the AFM sensor tip/cell surface contact events with cells. Both Raji-TSPAN33 and Raji-EGFP cells were independently placed over PLL or fibronectin to induce spreading, then fixed, and analyzed. During the measuring process, AFM cantilever moves with a constant spring rate generating indentation processes that are graphically interpreted as force *vs.* distance curves. At the beginning, the cantilever is brought closer to the membrane, finally indenting it and subsequently augmenting the force registered (Fig. 5C, upper left panel); later, the cantilever is retracted to its original position to generate a

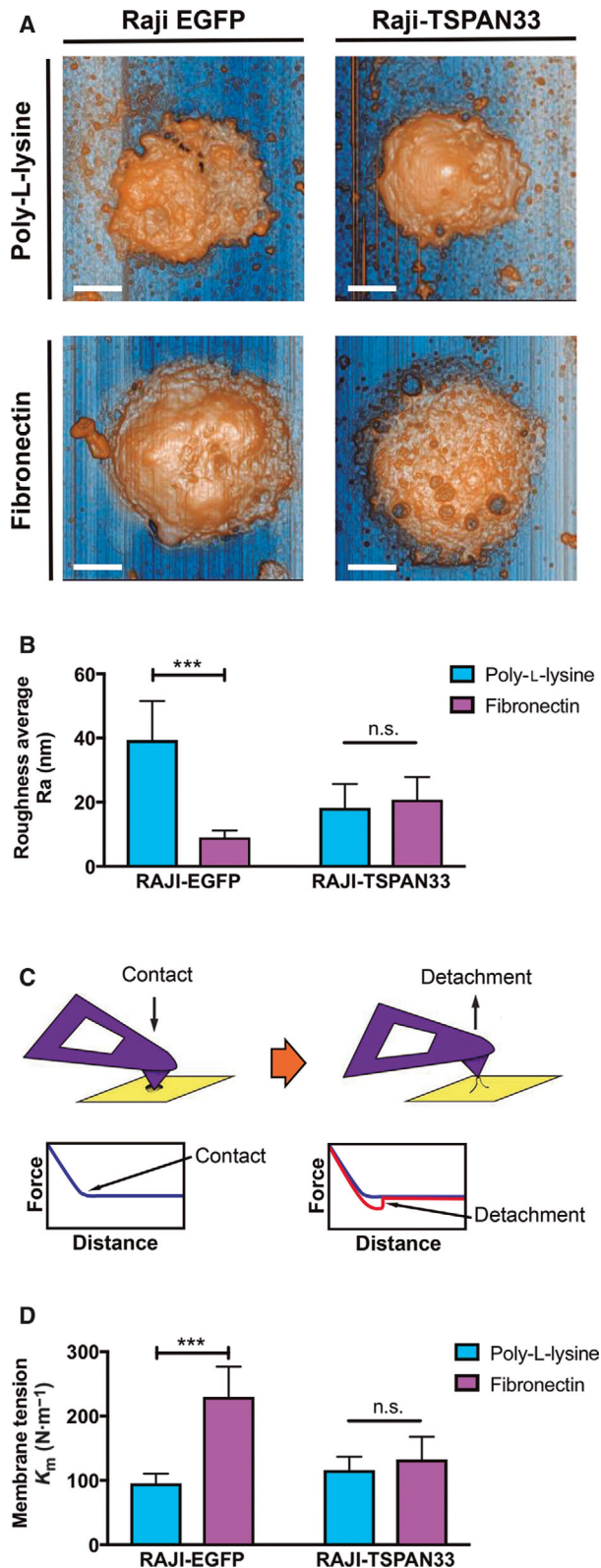


Fig. 5. TSPAN33 expression affects B-cell plasma membrane roughness and mechanical features. Raji-EGFP and Raji-TSPAN33 cells were adhered to PLL or fibronectin-coated coverslips and analyzed by AFM microscopy. (A) Cell surface roughness analysis. Representative 3D topography images are shown; bars represent 5 μ m. (B) Comparison of the roughness average values obtained; these values were calculated using the mean roughness of three sections in 10 cells from four independent measurements and presented as mean \pm SD; data were compared using a single-way ANOVA with a Bonferroni correction test *** $P \leq 0.001$. (C) Schematic representation during tip/surface contact and membrane indentation by the AFM cantilever in cell membranes, followed by a retraction (detachment) phase, where the tip generates a membrane tether with an equal force represented by deflections in the force vs. distance curves generated (schematically exemplified). Blue line shows the contact phase of the cantilever with the cell, and the red one represents the adhesion/detachment phase. (D) Membrane tension (K_m) values displayed were obtained from 20 cells in four independent measurements and presented as mean \pm SD; data were compared using a single-way ANOVA with a Bonferroni correction test *** $P \leq 0.001$.

membrane tether, which represents a retractive opposing force directly linked to the viscoelastic properties of the membrane, before full detachment of the tip (Fig. 5C, upper right panel). Accordingly, several experimental force *vs.* distance curves were obtained for individual cells of both lines (represented in Fig. 5C lower panels); these graphs show two curves, one for the contact phase (blue) and another for the detachment phase (red); both are nearly linear, but the magnitude of the deviation in the detachment slope can be directly correlated with membrane stiffness values. Once the elastic constants (K_m or membrane tension) were quantified following a mathematical approach previously reported by our group [53,54], we detected a ~ 2 -fold increase in this feature in control cells once spreading was induced over fibronectin when compared with cells incubated with PLL. Remarkably, TSPAN33-expressing cells did not exhibit any change in their membrane tension when they were put over both substrates (Fig. 5D). Altogether, these observations demonstrate that the presence/abundance of this tetraspanin can regulate the mechanic responses exerted by these leukocytes.

TSPAN33 interacts with ezrin in B lymphocytes

The interaction with cytoskeleton/membrane linkers, such as ERM proteins, is well documented for different tetraspanins [27,55]; as this protein–protein linkage could be regulating the observed membrane mechanical changes in our cells, we looked for evidence of

TSPAN33 interaction with the principal member of this class of proteins expressed by lymphocytes: ezrin.

First, we detected the distribution of ezrin in Raji-TSPAN33 cells by confocal microscopy. As shown in Fig. 6A, we found the colocalization of this linker protein with TSPAN33-EGFP in our cells. To determine whether TSPAN33 and ezrin are indeed associated, as suggested by confocal microscopy data, we performed

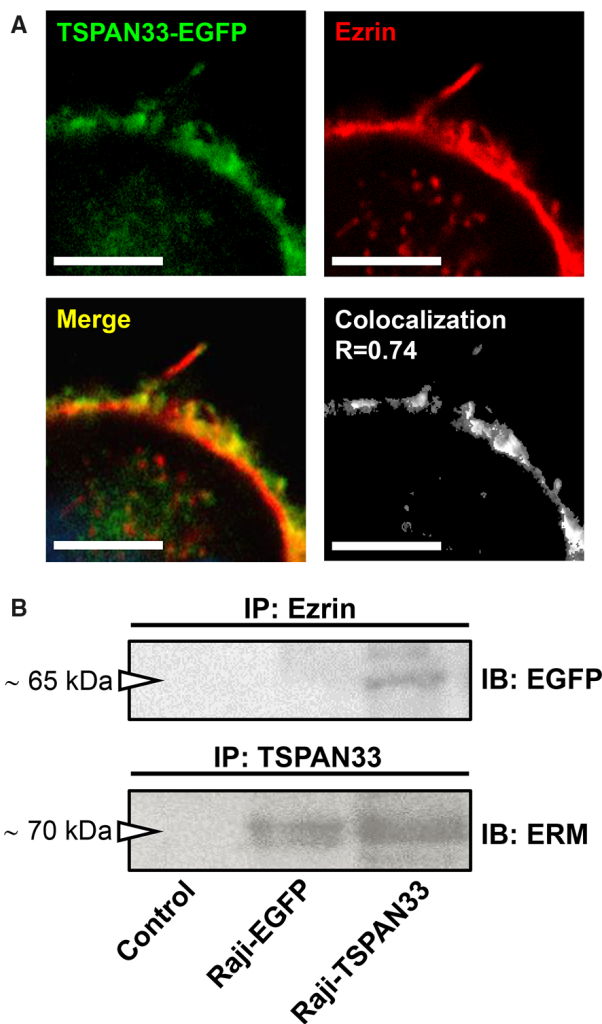


Fig. 6. TSPAN33 interacts with ezrin in B lymphocytes. (A) Confocal images of Raji-TSPAN33 cells (TSPAN33-EGFP, green) stained for ezrin (red); we appreciate the colocalization of these proteins (grayscale image) denoted as Pearson's correlation coefficient (R). The pictures shown are representative of three experiments performed. Bars represent 5 μm . (B) Lysates from Raji-EGFP and Raji-TSPAN33 cells were immunoprecipitated with either anti-ezrin or goat IgG (as isotype control), or anti-TSPAN33 or mouse IgG (as isotype control) plus Dynabeads Protein G. The beads were collected and mixed with Laemmli buffer before western blot analysis using anti-ERM or anti-GFP antibodies. The blots shown are representative of three independently performed.

a co-immunoprecipitation as described in Materials and methods. When we used anti-ezrin as a capture antibody, we detected the TSPAN33-EGFP fusion by anti-EGFP blotting (Fig. 6B, upper panel). Accordingly, if an anti-TSPAN33 was used for immunoprecipitation, we were able to detect the presence of ERM proteins (mainly ezrin but maybe also moesin or radixin, two very similar proteins) in both Raji-EGFP and Raji-TSPAN33 extracts (Fig. 6B, lower panel), thus corroborating that TSPAN33 and ezrin are interacting in both cell lines.

TSPAN33 knockdown promotes adhesion/phagocytosis but hinders B-cell migration

To validate our results obtained by overexpression of TSPAN33 and to demonstrate that the observed effects are directly derived from the presence of this tetraspanin, we decided to knock down its expression in Raji cells. We used a CRISPR-Cas9 approach to delete a genomic region between exons II and III of the *TSPAN33* gene (Fig. 7A, left panel). Although we were not able to obtain a TSPAN33-null expressing clone, we isolated a genomic edited cell clone named as Raji T33^{+/−} (Fig. 7A, right panel) that showed a close to 75% reduction in the total expression of TSPAN33 protein when compared with backbone vector-transfected WT cells, as measured by western blot (Fig. 7B).

Although no significant differences in the previously analyzed integrins were detected in both cell lines (data not shown), when we tested Raji T33^{+/−} cells' adhesive capacity over different substrates, we observed a significant increase in the extracellular matrix (ECM) adhesion of these when compared with WT cells (Fig. 7C).

Additionally, to corroborate the implication of TSPAN33 in phagocytosis, we performed assays using *E. coli*-pHrodo bacteria. We found that the partial ablation of TSPAN33 expression significantly promotes the phagocytic activity of these cells (Fig. 7D), thus confirming our previous observations.

We also found out that Raji T33^{+/−} cells exhibited significant differences in their chemotactic properties when compared to WT cells, as shown by their decreased Euclidean and accumulated migration distance values and their resulting lower absolute velocity, although there were no significant differences in their directionality (Fig. 7E). Furthermore, by performing our transwell invasion assay in Matrigel, we observed that Raji T33^{+/−} cells were significantly less capable of degrading and migrate (in response to CCL21) through the ECM than control cells (Fig. 7F). Again, we could not detect any significant difference in

CCR7 expression levels between Raji T33^{+/−} and WT cells (Fig. 7G).

Discussion

Tetraspanins regulate various molecular events through the organization and association with plasma membrane components, including their best-characterized partners such as integrins and MHC molecules [32,56]. Following this, an outstanding number of studies performed in nonimmune cells have demonstrated that widely expressed tetraspanins regulate adhesive properties of cells, implicating this phenomenon in a wide range of physiological and pathological processes. On the other hand, the number of studies assessing the implication of leukocyte-specific tetraspanins in migration and adhesion is limited [57,58]. TSPAN33 is an almost specific leukocyte tetraspanin, as shown by previous studies performed by our and other independent groups [35–37,40,59]. It is the last described member in the superfamily and forms part of the evolutionarily conserved TspanC8 subgroup, capable of directly associating with the membrane-anchored metalloprotease ADAM10, regulating its trafficking and function [60,61]. Although this observation was reported some years ago, no sustained biological effects in the absence of the protein and under homeostatic conditions have been reported [33,34]. Furthermore, to the extent of our knowledge, no study has been performed to analyze more functions of this mentioned C8 subgroup [32,56]. Thus, in this study, we describe for the first time the implication of the TSPAN33 in other tetraspanin-related functions apart from the trafficking of the mentioned protease [36].

Because of the initial lack of reliable antibodies for various experimental applications, we relied on the use of transgenic human B cells expressing a fluorescently tagged construct of TSPAN33 to study its cellular distribution, relating it with physiological functions such as cell adhesion. As shown in this study, microscopy observations show the TSPAN33 construct in actin-dependent structures known as microvilli; moreover, it was seen recruited to these structures and regulating its biogenesis. Even though no evidence of TSPAN33 (or other TspanC8) participating in direct cytoskeleton regulation is available, a proteomics study based on affinity capture coupled to mass spectrometry has shown interactions between human TSPAN33 and the ERM proteins ezrin and moesin [62,63]. Besides that, observations show that microvilli appearance or loss correlates with alterations in expression levels of the tetraspanins CD81 and CD82 [16,64]. Accordingly, the

phenotype of the Raji-TSPAN33 cells used in this study resembles that observed in the monocytic U937 cells overexpressing CD81; in fact, more abundant and longer microvilli were also noticed. Other tetraspanins have also been identified as microvilli residents in non-immune cells: CD82, TSPAN1, and TSPAN8 are present in vesicles secreted from the intestinal epithelial brush border, suggesting the presence of these molecules in the corresponding microvilli [65]; also, CD9 and CD63 are present in the microprotrusions of activated platelets and oocytes [66,67], thus suggesting that this tetraspanin property seems to be evolutionarily conserved in nature [68]. While we cannot rule out that the transgenic expression of TSPAN33 could affect the endogenous localization of this molecule, our results have consistently shown specific recruitment of this tetraspanin in B-cell microvilli; furthermore, this feature has been previously reported to help into the understanding of TspanC8 membrane dynamics [60]. Microvilli structures represent functional membrane domains in leukocytes where specific signaling and adhesion molecules are recruited to initiate and regulate normal and pathogenic cell interactions [69], processes in which we hypothesize TSPAN33 could be actively participating. Considering these data and previously denoted functions of other tetraspanin family members, we conclude that TSPAN33 represents a resident protein and an active regulator of B-cell microvilli; however, its biological implication in the regulation of other molecular partners is something pending to be reviewed.

Since different studies have demonstrated a clear implication of tetraspanins during the biogenesis of cell membrane protrusions, we also analyzed this using a fibronectin-induced cell spreading approach [53]. Cell-extension patterns observed between control cells and those with an excess of TSPAN33 were dramatically different since the latter develop a more polarized shape; moreover, filopodia-like protrusions extended over the substrate were significantly longer and wider than their control homologs, and lastly, adhered cells were surrounded by more abundant microvesicular structures. These spreading morphology patterns resemble those seen in prostate epithelial cells when CD82 transgenic expression is induced [70]. Explanations to these morphological changes induced by TSPAN33 aberrant expression could include the alterations in the surface-integrin repertoire and the consequently altered mechanical membrane features induced by TSPAN33, which in turn would modify actin cytoskeleton dynamics. However, the contribution of direct cytoskeleton regulators remains to be examined since several reports support the capacity of

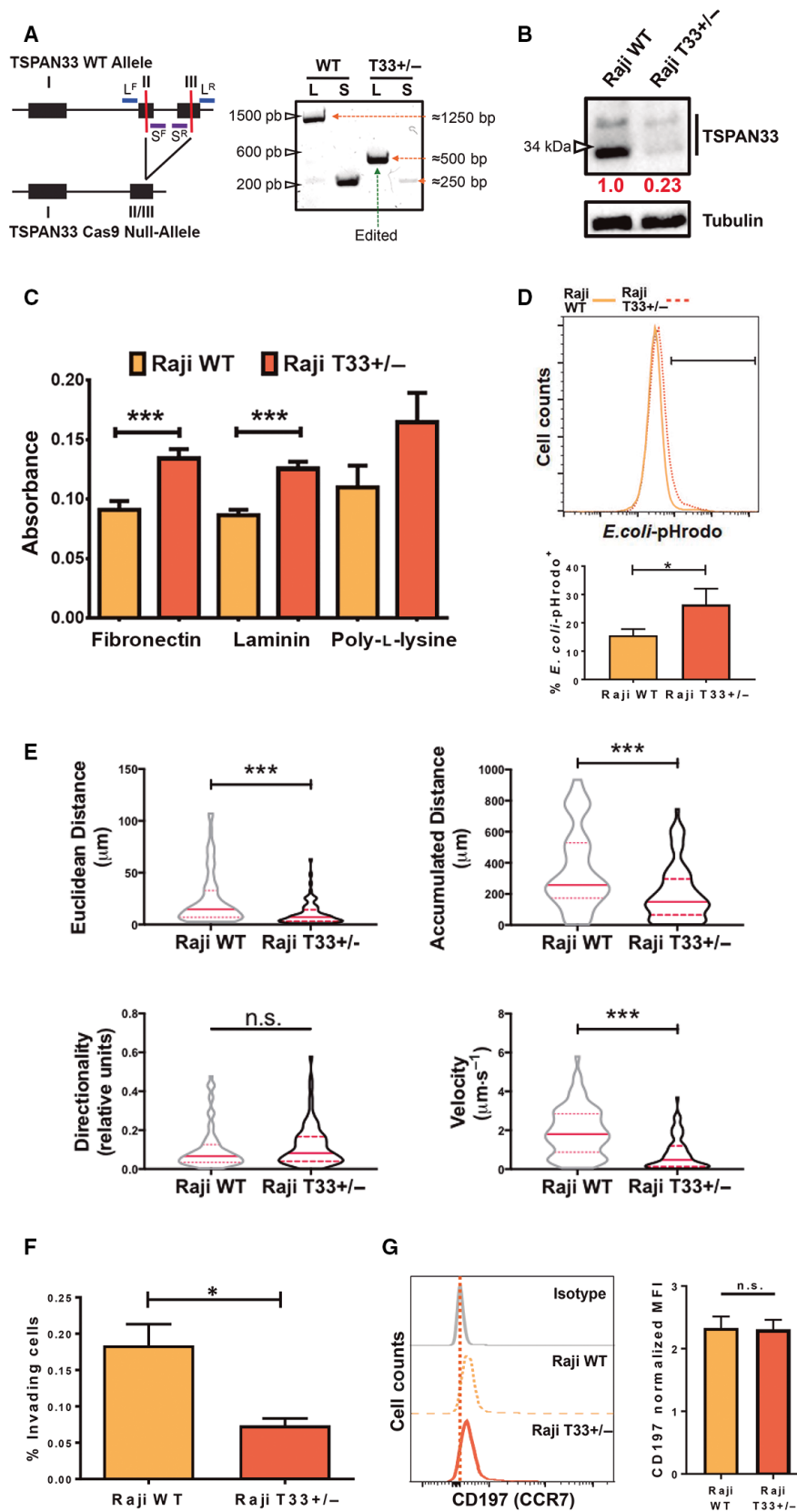


Fig. 7. TSPAN33 knockdown increases B-cell adhesion and phagocytosis. (A) TSPAN33 gene editing strategy. Schematic representation of the CRISPR-Cas9 approach used to delete a genomic region between *TSPAN33* exons II and III; genotyping primers designed are shown: The blue pair represents those that amplify the 'large' (L) 1261 bp amplicon, while the purple pair depicts those specific for the 'short' (S) 273 bp amplicon (left panel). The agarose gel on the right panel portrays the PCR analysis of the genomic region including exons II and III to corroborate the *TSPAN33* gene edition on the *T33^{+/−}* Raji cell clone, compared with WT cells, since the L amplicon was observed to be reduced to a ≈ 500 bp size and the almost lacking (but still detectable) S amplicon. (B) Western blot analysis for detection of TSPAN33 protein expression in Raji WT and Raji *T33^{+/−}* cells. Tubulin was used as loading control. Red numbers show the fold difference in expression of TSPAN33 (including both bands detected in each lane), once lanes were normalized against loading control as indicated in Materials and methods section. The blot shown is representative of two independently performed experiments. (C) Adhesion assays using Raji WT and Raji *T33^{+/−}* cells incubated with fibronectin, laminin, and PLL. Graph shows mean absorbance ± SD from three independent experiments. Data were analyzed using a single-way ANOVA with Bonferroni's *post hoc* test. ***P ≤ 0.001. (D) Phagocytosis assay using Raji WT and Raji *T33^{+/−}* cells incubated with *E. coli*-pHrodo. The results shown in the histogram are from one representative experiment. The graph shows the % *E. coli*-pHrodo (+) cells from three independent experiments. Data were analyzed using an unpaired two-tailed Student's *t*-test. *P ≤ 0.05. (E) Raji WT and Raji *T33^{+/−}* cells were placed over fibronectin-covered coverslips for 30 min; after that period, the coverslips were mounted in a Zigmond chamber to allow the cells to be exposed to a gradient of CCL21 and then capture their migration paths using a confocal microscope. The graphs show the Euclidean and accumulated distance, directionality, and velocity of these migratory cells. The values were originated from three independent experiments. Data are presented as mean (solid red line) plus lower and upper quartiles (dotted red lines) and were analyzed by an unpaired two-tailed Student's *t*-test. ***P ≤ 0.001. (F) Raji cells were placed in transwell upper chambers, previously covered with Matrigel; the cells were then exposed to a gradient of CCL21, for 16–18 h. The migrated cells in the lower chamber were then counted by flow cytometry. The graph shows the percentage of invading (migrated) cells regarding to total cells. The values were derived from three independent experiments. Data are presented as mean ± SD and were analyzed by an unpaired two-tailed Student *t*-test. *P ≤ 0.05. (G) Histograms showing expression of CCR7 (CD197) in Raji WT and Raji *T33^{+/−}* cell lines. The accompanier bar graph is derived from three independent tests; the normalized MFI ± SD is shown. These data were analyzed by an unpaired two-tailed Student's *t*-test.

tetraspanins to regulate the activity of small Rho GTPases [26,28,71–73] and ERM molecules, both implicated in the control of cytoskeletal rearrangements [27,55].

When we evaluated the attachment and migration capacity of Raji-TSPAN33 cells, we found a defect in their adhesive functions along with a reduced integrin surface expression; this effect was also accompanied by an enhanced capacity to follow a chemotactic CCL21 gradient, along with a more invasive phenotype; accordingly, all these outcomes were counteracted by partial ablation of TSPAN33 expression. As we mentioned before, the altered adhesion of these cells can be directly related to the modifications in the integrin repertoire; therefore, previous studies have shown that the adhesive properties of Burkitt lymphoma cells, including the Raji cell line, depend mainly on the expression of $\beta 1$ (CD29) integrins: the primary fibronectin receptor [74,75]. Also, a previous study from another group studying TspanC8-ADAM10 interactions found that three members of the subgroup (Tspan5, Tspan14, and Tspan15) physically associate with α subunits and with higher avidity with the β chains of the VLA-1, VLA-2, and VLA-3 integrins [60]. Alterations in the chemotactic ability of Raji-TSPAN33 were not surprising as they develop morphological phenotypes when spread over fibronectin, possibly due to the decreased adhesion mediated by these integrins, a property that seems to be reproduced by other leukocyte-specific tetraspanins like CD37

during inflammation, which exerts similar effects due to integrin recycling processes [76]. Additionally, another possible explanation for these effects is the altered mechano-sensing properties in TSPAN33-expressing cells, since previous reports have shown a relationship between this property and cellular motility. For example, changes in membrane tension of neutrophils represent a mechano-sensing feedback loop necessary for polarization and migration of these leukocytes [77]. Conversely, changes in membrane tension in nonimmune cells exert control on integrin ligand binding and activation during cell migration in a model termed 'molecular clutching,' but as denoted in these studies, the implication of other transmembrane molecules apart from integrins and their respective signaling molecules is not well defined [78–80]. In summary, data demonstrate that the expression of TSPAN33 can regulate integrin surface expression, and this property consequently modifies basic mechanical membrane features of leukocytes, which in turn could alter their adhesive and migration capacity.

Another exciting aspect upregulated in TSPAN33 transgenic cells but downregulated in TSPAN33-defective cells was its invasive capacity during 3D migration through ECM. Previous reports have established that invasion of tumor cells occurs via increased activity of invadopodia: a particular subtype of membrane protrusion where ECM-degrading proteases are recruited; accordingly, the formation of these structures correlates with some tetraspanin expression and represent

sites at which membranes undergo rapid recycling to promote vesicle secretion [81]. Following this, a molecular explanation for the behavior observed during 3D migration could be given by the classic interaction and regulation of ADAM10 protease by C8 tetraspanins. According to this, the additional amount of mature protease in the cell surface and the upregulation of its activity exerted by TSPAN33 could hypothetically promote direct ECM degradation in a process that could be potentiated by reported changes in the mechanic properties of the cell membrane [61]. In addition, we cannot discard that this migratory phenotype could also be the result of altered vesicular trafficking and secretion; following this, TSPAN33-containing EV could enhance the migration capacity of normal and malignant B cells through a yet unknown mechanism [82]. On this regard, EV-induced migration/metastasis has already been related to the presence of other tetraspanins like CD82, which is capable of inhibiting laminin adhesion and migration, or CD9 that promotes the recruitment of CD10 (a protease implicated in B-cell maturation and migration) in exosomes [83,84]. So, the TSPAN33 presence in EVs, the upregulated production of these structures by TSPAN33 transgenic cells, and the localization of the protein in trans-Golgi compartments support our previous statements, although further work is necessary to understand the role of this tetraspanin in vesicular dynamics.

Another way to evidence alterations in membrane properties is by measuring changes in their endocytosis rate [85]. Phagocytosis is one of the most evolutionarily conserved functions in pluricellular organisms and is a vital component of immunity shared by TSPAN33-expressing leukocytes, such as B cells and macrophages [86]. Although B cells are not typically seen as phagocytic cells, our and other independent groups have shown that human B lymphocytes develop this process to engulf different particles such as bacteria (i.e., *Salmonella* spp., *Mycobacterium* spp., or *Staphylococcus aureus*) [36,43]. Furthermore, recent studies have started to elucidate different molecular mechanisms used by leukocytes and other cell types to develop phagocytosis, establishing integrins as one of the most studied molecule families linked with this phenomenon [87]. In this regard, VLA integrins bind different targets from *Yersinia* spp., *E. coli*, *S. aureus*, *Shigella* spp., human cytomegalovirus, and herpes virus, among other pathogens [88]. Accordingly, when we used different fluorescent *E. coli* bacteria to study phagocytosis, we detected impaired activity when TSPAN33 was overexpressed, an observation that correlates with CD29 surface levels. Moreover, the inverse

phagocytic effect is observed when this tetraspanin is partially ablated in Raji cells.

Additionally, if membrane tension is altered, one of the principal cellular features affected is the endocytic–exocytic equilibrium [85]. Frustrated phagocytosis assays in fibroblasts demonstrated that pseudopod extension, necessary for phagocytic engulfment, occurs in two phases: The first one is fast and supported mainly by actin polymerization, and the second depends on an increase in membrane tension. This transient increase in tension alters the localization pattern of protrusion regulator molecules including activated Rac1, phosphatidylinositol (3,4,5)-trisphosphate, and actin [20]. Considering that increased levels of TSPAN33 decreased the adhesion to ECM, we hypothesize that these cells present an impairment to develop the required transient increase in local membrane tension, thus reducing its effective phagocytic ability. Concomitantly, the diminished tetraspanin level in knockdown cells slightly enhances this same endocytic phenomenon, probably as a result of altered recruitment and function of the mentioned membrane protrusion-forming regulators.

The coupling of biochemical events with mechanical stimuli such as integrin ligand binding and actin polymerization is crucial for the whole membrane remodeling processes during cell adhesion; however, the implication of other transmembrane molecules remains unclear [80,89,90]. As mentioned, membrane tension is an essential regulator of many eukaryotic cell processes such as migration, division, endocytosis–exocytosis, osmoregulation, and cell spreading [11,91,92]. The total surface tension of the plasma membrane is defined by different elements that include the intrinsic surface tension of the lipid bilayer, adhesion processes that cells could be established with the surrounding environment, and, most importantly, the molecular connection between the membrane and the underlying actin cytoskeleton cortex [93]. Accordingly, there is much evidence indicating that membrane tension in eukaryotic cells could be regulated by cytoplasmic proteins linking the plasma membrane and cytoskeleton, such as unconventional class I myosins [53] or members of the ERM family [94,95]. The contribution to this membrane property of other protein families, particularly those possessing transmembrane domains, has been mainly associated with adhesion molecules such as integrins [96] that are indirectly connected to the plasma membrane-underlying actin cortex of cells by the referred cytoplasmic linker proteins. Interestingly, it has been reported that the altered expression levels or function of these linker proteins can affect biophysical membrane-related parameters and, consequently,

effector functions of B lymphocytes, including antigen discrimination and processing [10,53,97].

A remarkable attribute of Raji-TSPAN33 cells is their altered membrane roughness when attachment to fibronectin takes place. Average roughness of cells indicates an adequate link between the cytoskeleton and the plasma membrane resulting from the regulation of membrane tension [98]. Cell surface roughness contributes to cellular processes such as migration and the regulation of cellular contacts [91], for example, a correlation between high cell roughness and high invasiveness was seen in MCF7 cells when compared with their smooth noninvasive MCF10 counterparts [99]. Several molecules have been related to the maintaining of cell roughness, but no reports linking tetraspanins with this attribute emerged until now. Remarkably, the data presented in this study show that TSPAN33 expression level is affecting the plasma membrane tension of Raji B cells, a feature that seems to be impacting in all the membrane-related processes analyzed.

All data showed here demonstrate a link between TSPAN33 and cell surface dynamics, but how its expression levels explicitly affect membrane and cytoskeleton properties regulating the different cell functions depicted in this work remains partially unclear. One important observation that could functionally explain what we observed is the detected interaction of TSPAN33 with ezrin, a protein that, as explained before, is responsible for connecting the cytoskeleton with the plasma membrane, thus directly regulating its mechanical properties and its consequent functionality. Whether TSPAN33 is controlling ezrin recruitment or activation processes is not clear yet, but that emerges as an attractive possibility that could confer to this tetraspanin a preponderant role during membrane rearrangement processes in leukocytes.

Along with the previously detailed observations, we can also speculate around the role of TSPAN33 in maintaining the stability and composition of TEMs. Besides the documented tetraspanin partnership with other proteins, there is evidence about the interaction of tetraspanins with some lipid components of the plasma membrane such as cholesterol [24] or gangliosides [100]. Fascinatingly, it is reported that the expression of tetraspanin CD82 in epithelial cells correlates with the increased surface expression of gangliosides GD1a and GM1 [101], and also, in fibroblasts the cell binding to fibronectin leads to a rise in cholesterol synthesis [102]. Considering these data, it is also possible that alterations in the expression of TSPAN33 could be affecting the composition of TEMs and other microdomains in the plasma membrane of Raji cells, inducing changes in the repertoire of surface proteins

and membrane lipids. Therefore, TSPAN33 levels could be affecting their functional properties in two different ways: first, biochemically, since these micro-domains can recruit and regulate the activation of cytoskeletal linkers such as ERM proteins, or biophysically since the high content of lipids like cholesterol confers more stiffness to the membrane regions where it is included [103]. In addition, the fact that some tetraspanins can control the lateral diffusion of proteins, thus regulating the clustering of the transmembrane proteins they interact [33], represents a feature that serves to modulate its activation. This last idea is relevant since it can also be useful to explain our observations about the adhesion alterations in the Raji-TSPAN33 and Raji T33^{+/−} cells.

Altogether, data showed here give the first insights into how TSPAN33 expression globally changes the adhesive and endocytic capacity of B cells and how it modulates its response to chemotactic stimuli during 2D and 3D substrate migration. Moreover, these observations are crucial in understanding the implication of these tetraspanins beyond their specific associations, in which some immunotherapeutic-targeting proposals are based, and raise the possibility that these treatments could have unexpected outcomes derived from these alternative functions. The results reported in this paper also provide evidence of the participation of TSPAN33 in the modulation of the plasma membrane and associated underlying cytoskeleton dynamics that affect different cellular processes that B cells can develop during activation including endocytosis/phagocytosis, adhesion, and different migration variants. Further studies are necessary to understand the role of TSPAN33 in cytoplasmic/extracellular vesicular trafficking/secretion and its implication for the reorganization of plasma membrane components, where this molecule seems to be an active player.

Materials and methods

Cells and reagents

B-cell experiments were performed using the Raji cell line (ATCC, Manassas, VA, USA, cat. ATCC CCL-86), obtained from human neoplastic tissue of Burkitt lymphoma. Also, established clones of Raji transfected with EGFP and TSPAN33-EGFP [36] were used. All cell cultures were maintained in RPMI-1640 medium (Gibco, Waltham, MA, USA, cat. 21875091) with 10% FBS (Gibco cat. 10437028), 100 U·mL^{−1} penicillin, 100 µg·mL^{−1} streptomycin, 0.3 mg·mL^{−1} L-glutamine, and 1 mM sodium pyruvate (Gibco cats. 10378016 and 11360070) at 37 °C with 5% CO₂. Other reagents used were WGA Alexa Fluor 555

(Molecular Probes, Waltham, MA, USA, cat. W32464, 5 µg·mL⁻¹), lectin GSII from *G. simplicifolia* Alexa Fluor 594 (Molecular Probes cat. L21416, 5 µg·mL⁻¹), TRITC-phalloidin (Molecular Probes cat. 10063052, 1 : 600), fibronectin (Takara Bio., Mountain View, CA, USA, cat. T100B, 2.5 ng·µL⁻¹), laminin from Engelbreth-Holm-Swarm murine sarcoma basement membrane (Sigma-Aldrich, St. Louis, MO, USA, cat. L2020, 5 ng·µL⁻¹), recombinant human CCL21 (R&D Systems, Minneapolis, MN, USA, cat. 966-6C-025CF, 10 ng·mL⁻¹), Matrigel Matrix (Corning, Corning, NY, USA, cat. 354234), and p^{CMV}LifeAct-TagRFP (Ibidi, Gräfelfing, Germany, cat. 60102).

Confocal microscopy

For immunofluorescence staining, the cells were washed with PBS and fixed for 15 min with 4% paraformaldehyde (PFA; Sigma-Aldrich cat. 158127), permeabilized with 0.1% of Triton X-100 (Sigma-Aldrich cat. X100), and incubated with the different fluorescent reagents before mentioned as described previously in Ref. [41]. For the detection of ezrin, anti-human ezrin (Santa Cruz Biotechnology, Dallas, TX, USA, cat. sc-6407, 1 : 200) was used. For live-cell observations, the cells were put into bottom glass Petri dishes (NEST, Jiangsu, China, cat. 801002) containing supplemented RPMI-1640 medium. The preparations were then analyzed with an Olympus microscope using 60× objectives and the Olympus FluoView or NIH IMAGEJ software (NIH, Bethesda, MD, USA) for measurements and correlation coefficient calculations.

Scanning (SEM) and transmission (TEM) electron microscopy

For SEM, cells were fixed with 2% (v/v) glutaraldehyde (Sigma-Aldrich cat. G5882) in 0.1 M cacodylate (Sigma-Aldrich cat. C0250) buffer, pH 7.2, and dehydrated with increasing concentrations of ethanol. Samples were critically point-dried in a Samdri apparatus, gold-coated with an ion-sputtering device (Jeol JFC-1100), and examined with a Jeol JSM-7100F field-emission scanning electron microscope. For TEM, cells or extracellular vesicle preparations were fixed in PFA 4% and glutaraldehyde 0.1% in serum-free RPMI-1640 medium for one h at room temperature. Samples were embedded in LR White (Sigma-Aldrich cat. 62661) and polymerized under UV at 4 °C overnight. Sections were obtained and mounted on formvar (Sigma-Aldrich cat. 09823)-covered nickel grids. Thin sections were observed in a Jeol JEM-1011 microscope.

Microvilli isolation and western blot analysis

Raji B cells (1×10^9) were suspended in PBS containing 20% FBS and incubated for 20 min at 37 °C. Cells were passed through a 27^{1/2}G needle five times to shear off the microvilli. The samples were centrifuged as described

previously in Ref. [104] for the isolation of membrane/microvilli fraction (MMV) and the postnuclear lysate (PNL) fraction. The monoclonal antibodies used for conventional western blot detection are anti-human actin (Santa Cruz Biotechnology cat. sc-8432, 1 : 800), anti-human β tubulin (Santa Cruz Biotechnology cat. sc-55529, 1 : 500), anti-human ezrin (Santa Cruz Biotechnology cat. sc-6407, 1 : 500), anti-human nucleoporin p62 (Santa Cruz Biotechnology cat. sc-48373, 1 : 200), anti-GFP (Thermo Fisher Scientific, Waltham, MA, USA, cat. A-11120, 1 : 500), and the secondary detection antibody anti-mouse IgG-HRP (Zymed, Waltham, MA, USA cat. 31430, 1 : 10 000). Also, for western blot detection of both endogenous TSPAN33 or the EGFP-tagged fusion protein, the antibodies rabbit anti-human TSPAN33 (Biorbyt, Cambridge, UK, cat. orb40093, 1 : 250) and anti-rabbit IgG-HRP (Zymed, cat. 31460, 1 : 10 000) were used.

Spreading assays

Glass slides were coated with fibronectin in PBS for 1 h at 37 °C. The coverslips were blocked with PBS containing 10% FBS for 1 h at 37 °C and then washed thoroughly with the medium before use. Raji cells line were transferred without washing to the precoated glass slides and incubated for 2 h at 37 °C. The cells were then treated, as described previously [41].

Extracellular vesicles isolation

Ten milliliter of cell cultures supernatants was filtered through a sterile syringe filter of 0.2 µm and was incubated for 24 h with 2 mL of PEG8000 (Sigma-Aldrich cat. 89510, 5 mg·mL⁻¹) in PBS at 4 °C. The samples were then centrifuged at 1500 g for 30 min at 4 °C. The pellet was recovered and resuspended with 200 µL of sterile PBS. The vesicle-enriched fractions obtained were then analyzed by TEM and conventional SDS/PAGE and western blot using a rabbit anti-GFP (Invitrogen, Waltham, MA USA, cat. A-11122, 1 : 500) and anti-rabbit IgG-HRP (Zymed cat. 31460, 1 : 10 000).

Adhesion assays

Polystyrene plates were coated with various substrates such as PLL (Sigma-Aldrich cat. P8920, 0.01%), fibronectin (Takara Bio. cat. T100B, 2.5 ng·µL⁻¹), and laminin (Sigma-Aldrich cat. L2020, 5 ng·mL⁻¹) for 1 h at 37 °C. The plates were then washed twice with PBS before adding 5×10^4 Raji cells in 200 µL of RPMI-1640 per well. After cells were incubated for 1 h at 37 °C, then, the plates were washed with 300 µL of PBS and fixed with 4% PFA for 10 min before adding Crystal Violet (7.5 g·L⁻¹, NaCl 2.5 g·L⁻¹, formaldehyde 1.57%, methanol 50%) for an additional 5 min. After that, these cells were washed thoroughly three times with distilled water and solubilized with

10% SDS (Sigma-Aldrich cat. L3771). Finally, plates were read at 540 nm using an xMark™ microplate absorbance spectrophotometer (Bio-Rad, Hercules, CA, USA). The absolute binding was obtained after subtracting the non-specific colorimetric readings from the absorbance for each well. The data were analyzed with the results of three independent experiments using three wells per condition.

Flow cytometry

A total of 5×10^5 cells in suspension were collected by centrifugation. The pellet was suspended in PBS and incubated at 4 °C with anti-human CD18-PeCy5 (BioLegend, San Diego, CA USA, cat. 302109, 5 µL/1 $\times 10^6$ cells) and anti-human CD29-PeCy5 (BioLegend cat. 303006, 5 µL/1 $\times 10^6$ cells) for 20 min. Then, cells were then washed with PBS and fixed with 4% PFA. Finally, the cells were suspended in PBS and analyzed in an LSRFortessa flow cytometer (BD Biosciences, San Jose, CA USA). The data obtained were processed with the FLOWJO software (BD Biosciences).

Migration assay

The evaluation of migration was performed using a Zigmond chamber as described in Ref. [41] with the addition of recombinant human CCL21 (R&D Systems cat. 966-6C-025CF, 10 ng·mL⁻¹) in supplemented RPMI-1640. The migration data were recorded and analyzed with NIH IMAGEJ software. Data were obtained from three to four independent experiments following the migration tracks of at least 100 lymphocytes of each cell line.

Invasion assay

Briefly, the stock of Matrigel Matrix (Corning cat. 354234) was thaw overnight at 4 °C and then diluted 1 : 1 with RPMI-1640 medium. 70 µL of liquid Matrigel was then placed directly on the center of the 8 µm polycarbonate transwell inserts in 24-well plates (Thermo Fisher Scientific-Nunc cat. 140629). The plates were put in a humidified incubator at 37 °C for at least 3 h. Meanwhile, 1 $\times 10^5$ cells of any Raji cell line were washed and suspended in 200 µL of RPMI-1640 medium and added to each of the upper compartments (inserts). The lower chambers (plate wells) were filled (500 µL) with RPMI-1640 medium with or without CCL21 at the previously indicated concentration. The plates were then placed at 37 °C for 24 h to allow cells to invade through the Matrigel. Finally, the lower chamber content was collected, washed, and suspended in 1 mL of PBS to count the cells in an Accuri C6 flow cytometer (BD Biosciences).

Phagocytosis

For *in vitro* assessment of phagocytosis, Raji cells were incubated with *E. coli*-RFP or pHrodo-Red *E. coli*

BioParticles (Thermo Fisher Scientific cat. P35361, bacteria-to-cell ratio 10 : 1) in 24-well plates with 100 µL of supplemented RPMI-1640 medium, for 3 h at 37 °C in 5% CO₂. Then, cells were harvested and washed with cold PBS before the addition of 0.5 mL of a quenching trypan blue solution (Sigma-Aldrich cat. 302643, 50 µg·mL⁻¹) as described previously [43]. The cells were fixed with 4% PFA for 15 min. Finally, cells were washed with PBS and analyzed by flow cytometry in a LSRFortessa flow cytometer (BD Biosciences) or mounted in VECTASHIELD (Vector Laboratories, Burlingame, CA, USA, cat. H-1000-10) and observed using a TCS SP8 confocal microscope (Leica Microsystems, Wetzlar, Germany) using 63× objectives and analyzed with LAS AF LITE software (Leica Microsystems).

Measurement of cell stiffness and topography

We used the XE-Bio AFM (Park Systems, Suwon, Korea) to estimate the elasticity of the cells. We measured the spring constant of the cells, considering the methodology depicted in Ref. [53]. Briefly, a silicone-nitride pyramidal tip cantilever (Bruker, Camarillo, CA, USA), with a nominal spring constant of 60 mN·m⁻¹, was used to obtain topographic images. Independently, one highly doped silicon (NCHR) pyramidal tip cantilever, with a nominal spring constant of 42 N·m⁻¹ (Nanosensors, Neuchâtel, Switzerland), was used to obtain force *vs.* distance curves. Topographic images, as well as force *vs.* distance curves of fixed cells, were obtained in the air at 20 °C, in contact mode using scanning frequencies between 1 and 3 Hz. All elasticity measurements were less than 100 nm in depth. Approach and retraction velocities were between 3 and 5 µm·s⁻¹. A total of 20 cells were measured for each cell line analyzed.

Specific features in the AFM topography were analyzed by line profiling routines provided in the WSXM imaging software (www.wsxm.es). The roughness of at least three aleatory selected regions of each cell analyzed was measured relative to the surrounding membrane (not the substrate). Because the cell membranes are irregularly shaped, care was taken for each zone in acquiring representative profiles. The profiles were then analyzed using the WSXM imaging software to obtain several graphs and values of roughness. All the membrane tension and roughness mean values data were processed with PRISM 8 software (GraphPad Software, San Diego, CA, USA) for statistical analysis.

Co-immunoprecipitation analyses

Raji-EGFP or Raji-TSPAN33 cells (1 $\times 10^8$) were washed with cold PBS and lysed for 30 min on ice in 1% Triton X-100 in TNE buffer containing protease and phosphatase inhibitors [10 mM Tris/HCl (pH 7.5), 150 mM NaCl, and 5 mM EDTA plus 2.5 mg·mL⁻¹ each of PMSF, leupeptin,

aprotinin in DMSO, and 1 mM sodium orthovanadate]. The mixture was further homogenized with ten strokes in a glass Wheaton loose-fitting Dounce homogenizer. Cell debris was pelleted by centrifugation 10 min at 900 g. The extracts were co-immunoprecipitated using either anti-human ezrin (Santa Cruz Biotechnology cat. sc-6407, 2 µg) and goat IgG (Sigma-Aldrich cat. I5256) as the isotype control, or mouse anti-human TSPAN33 (BioLegend cat. 395402, 2 µg) and mouse IgG (Sigma-Aldrich cat. I5381) as an isotype control. The reactions were incubated for four h, and then, complexes were precipitated using Dynabeads Protein G beads (Thermo Fisher Scientific cat. 10007D) maintaining the temperature at 4 °C during all procedures. Beads were washed with cold TNE and boiled in sample buffer. SDS/PAGE and western blot analysis were performed according to standard protocols, blotting for TSPAN-EGFP and ERM, using rabbit anti-GFP (Invitrogen cat. A-11122, 1 : 500) or rabbit anti-human ERM (Abcam, Cambridge, UK, cat. ab231642, 1 : 200) plus anti-rabbit IgG-HRP (Zymed cat. 31460, 1 : 10 000).

TSPAN33 knockdown generation

The CRISPR/Cas9 system was used for the generation of a TSPAN33-deficient Raji cell clone, using two nonoverlapping guide RNA pairs targeting exons 2 (5'-TGCTGTGGGTGTCTACGCTCGG-3') and 3 (5'-GAGGCAGATGTTCTCCGGAGGG-3') from the TSPAN33 gene (ENST00000486685.2). The guides were designed and analyzed using the CRISPOR web tool [105] and subcloned into the pSpCas9(BB)-2A-GFP (PX458) vector, as described previously [106]. Shortly, Raji cells were transfected with one ug of each recombinant plasmids or empty vector backbone, using the Neon electroporation system (Thermo Fisher Scientific), following a protocol of two 1350 V pulses with a duration of 20 ms each. Two days after electroporation, Cas9-positive single cells were isolated from the bulk culture by using a FACSaria III flow cytometer (BD Biosciences) into 96-well plates. After 15–25 days of culture, we could only retrieve 22 stable clones that were screened for genomic deletions applying a PCR approach described previously [106], by using the primers 5'-GCAGAGAGTCATCAAGGGCT-3' and 5'-GTTAAGGGGAGGCAGTACCC-3' for a large amplicon (1261 bp) flanking exons II and III (large = L), and 5'GGGGAGGTGAAAGATGCTCA-3' and 5'-GTCTAG-GACCACTCATGGCA-3' for a smaller amplicon (273 bp) inside the intron between exons II and III (short = S) (Fig. 7A). By this method, we detected 19 edited clones that were checked for TSPAN33 expression by western blot procedures using rabbit anti-human TSPAN33 (Abcam cat. ab87543, 1 : 500) and anti-rabbit IgG-HRP (Zymed cat. 31460, 1 : 10 000). We did not obtain any knockout cell clone, but we recovered one viable cell clone (named as Raji T33^{+/−}) displaying a ~75% reduction in TSPAN33

expression (Fig. 7B) that was used for the experiments shown.

Normalization of densitometry data

After western blot resulting band intensity was determined by densitometry IMAGEJ (NIH) integrated plug-in, the control protein (tubulin) was used to normalize TSPAN33 protein expression by multiplying the density of the TSPAN33 in each lane by the ratio of loading control density from the control sample (first lane: Raji-EGFP or WT cells) to the loading control density of other lanes. The fold change was then calculated by dividing the normalized expression from each lane by the normalized expression of the control sample in the first line of each blot.

Statistical analysis

For results analysis, PRISM 8 (GraphPad Software) software was used. Results are shown as the mean ± standard deviation (SD). An unpaired two-tailed Student's *t*-test or ANOVA was used to assess the statistical significance of differences between the Raji-EGFP and Raji-TSPAN33 groups. The *P*-values obtained and the number of samples or cells (*n*) used are stated in each figure legend.

Acknowledgements

This work was supported by grants CB 240314 and A3-S-36875 from CONACyT and IA204316, IA202318, IN213020, and IG100920 from UNAM-DGAPA-PAPIIT Program. NH-I was supported by fellowships 420255 and 587790 from CONACyT. The authors want to thank Zayda Piedra Quintero for her help with flow cytometry; Alfonso Felipe-López for the *E. coli*-RFP bacteria strain; Ismael Martínez-Cortés for the Matrigel donation; and Héctor Romero-Ramírez and Julio García-Cordero for their technical assistance.

Conflict of interest

The authors declare no conflict of interest.

Author contributions

IN-H, OL-O, EA-O, RC-D, SR-R, VS-H, and JM-M contributed to the experimental design, contributed to all the experiments, and wrote the paper. CP-M and DM-S contributed to microvilli analyses and cell line maintenance. GJ-V contributed to flow cytometry procedures. BM-C performed the EM captures. AG-H, AA, and IO-B performed, analyzed, and interpreted

the AFM measurements. LS-A, JH-H, and JM-M contributed to technical and/or financial resources. JM-M supervised the work.

References

- 1 Parsons JT, Horwitz AR & Schwartz MA (2010) Cell adhesion: integrating cytoskeletal dynamics and cellular tension. *Nat Rev Mol Cell Biol* **11**, 633–643.
- 2 Bromley SK, Burack WR, Johnson KG, Somersalo K, Sims TN, Sumen C, Davis MM, Shaw AS, Allen PM & Dustin ML (2001) The immunological synapse. *Annu Rev Immunol* **19**, 375–396.
- 3 Carrasco YR, Fleire SJ, Cameron T, Dustin ML & Batista FD (2004) LFA-1/ICAM-1 interaction lowers the threshold of B cell activation by facilitating B cell adhesion and synapse formation. *Immunity* **20**, 589–599.
- 4 Grakoui A, Bromley SK, Sumen C, Davis MM, Shaw AS, Allen PM & Dustin ML (1999) The immunological synapse: a molecular machine controlling T cell activation. *Science* **285**, 221–227.
- 5 Springer TA (1990) Adhesion receptors of the immune system. *Nature* **346**, 425–434.
- 6 Tolar P (2017) Cytoskeletal control of B cell responses to antigens. *Nat Rev Immunol* **17**, 621–634.
- 7 Ley K, Laudanna C, Cybulsky MI & Nourshargh S (2007) Getting to the site of inflammation: the leukocyte adhesion cascade updated. *Nat Rev Immunol* **7**, 678–689.
- 8 Kinashi T (2005) Intracellular signalling controlling integrin activation in lymphocytes. *Nat Rev Immunol* **5**, 546–559.
- 9 Lagarrigue F, Kim C & Ginsberg MH (2016) The Rap1-RIAM-talin axis of integrin activation and blood cell function. *Blood* **128**, 479–487.
- 10 Olety B, Walte M, Honnert U, Schillers H & Bahler M (2010) Myosin 1G (Myo1G) is a haematopoietic specific myosin that localises to the plasma membrane and regulates cell elasticity. *FEBS Lett* **584**, 493–499.
- 11 Sheetz MP & Dai J (1996) Modulation of membrane dynamics and cell motility by membrane tension. *Trends Cell Biol* **6**, 85–89.
- 12 Giri A, Bajpai S, Trenton N, Jayatilaka H, Longmore GD & Wirtz D (2013) The Arp2/3 complex mediates multigeneration dendritic protrusions for efficient 3-dimensional cancer cell migration. *FASEB J* **27**, 4089–4099.
- 13 Guerrier S, Coutinho-Budd J, Sassa T, Gresset A, Jordan NV, Chen K, Jin WL, Frost A & Polleux F (2009) The F-BAR domain of srGAP2 induces membrane protrusions required for neuronal migration and morphogenesis. *Cell* **138**, 990–1004.
- 14 Houk AR, Jilkine A, Mejean CO, Boltysanskiy R, Dufresne ER, Angenent SB, Altschuler SJ, Wu LF & Weiner OD (2012) Membrane tension maintains cell polarity by confining signals to the leading edge during neutrophil migration. *Cell* **148**, 175–188.
- 15 Ladwein M & Rottner K (2008) On the Rho'd: the regulation of membrane protrusions by Rho-GTPases. *FEBS Lett* **582**, 2066–2074.
- 16 Quast T, Eppler F, Semmling V, Schild C, Homsi Y, Levy S, Lang T, Kurts C & Kolanus W (2011) CD81 is essential for the formation of membrane protrusions and regulates Rac1-activation in adhesion-dependent immune cell migration. *Blood* **118**, 1818–1827.
- 17 Windus LC, Claxton C, Allen CL, Key B & St John JA (2007) Motile membrane protrusions regulate cell-cell adhesion and migration of olfactory ensheathing glia. *Glia* **55**, 1708–1719.
- 18 Worthylake RA & Burridge K (2003) RhoA and ROCK promote migration by limiting membrane protrusions. *J Biol Chem* **278**, 13578–13584.
- 19 Yamashiro S, Yamakita Y, Ono S & Matsumura F (1998) Fascin, an actin-bundling protein, induces membrane protrusions and increases cell motility of epithelial cells. *Mol Biol Cell* **9**, 993–1006.
- 20 Masters TA, Pontes B, Viasnoff V, Li Y & Gauthier NC (2013) Plasma membrane tension orchestrates membrane trafficking, cytoskeletal remodeling, and biochemical signaling during phagocytosis. *Proc Natl Acad Sci USA* **110**, 11875–11880.
- 21 Wang W, Tao K, Wang J, Yang G, Ouyang Q, Wang Y, Zhang L & Liu F (2017) Exploring the inhibitory effect of membrane tension on cell polarization. *PLoS Comput Biol* **13**, e1005354.
- 22 Basu R, Whitlock BM, Husson J, Le Floc'h A, Jin W, Oyler-Yaniv A, Dotiwala F, Giannone G, Hivroz C, Biais N *et al.* (2016) Cytotoxic T cells use mechanical force to potentiate target cell killing. *Cell* **165**, 100–110.
- 23 He HT & Bongrand P (2012) Membrane dynamics shape TCR-generated signaling. *Front Immunol* **3**, 90.
- 24 Charrin S, Manie S, Thiele C, Billard M, Gerlier D, Boucheix C & Rubinstein E (2003) A physical and functional link between cholesterol and tetraspanins. *Eur J Immunol* **33**, 2479–2489.
- 25 Franz J, Tarantola M & Riethmuller C (2017) How tetraspanins shape endothelial and leukocyte nano-architecture during inflammation. *Biochem Soc Trans* **45**, 999–1006.
- 26 Arnaud MP, Vallee A, Robert G, Bonneau J, Leroy C, Varin-Blank N, Rio AG, Troadec MB, Galibert MD & Gandemer V (2015) CD9, a key actor in the dissemination of lymphoblastic leukemia, modulating CXCR4-mediated migration via RAC1 signaling. *Blood* **126**, 1802–1812.
- 27 Coffey GP, Rajapaksa R, Liu R, Sharpe O, Kuo CC, Krauss SW, Sagi Y, Davis RE, Staudt LM, Sharman JP *et al.* (2009) Engagement of CD81 induces ezrin

- tyrosine phosphorylation and its cellular redistribution with filamentous actin. *J Cell Sci* **122**, 3137–44.
- 28 Hong IK, Jeoung DI, Ha KS, Kim YM & Lee H (2012) Tetraspanin CD151 stimulates adhesion-dependent activation of Ras, Rac, and Cdc42 by facilitating molecular association between beta1 integrins and small GTPases. *J Biol Chem* **287**, 32027–32039.
- 29 Johnson JL, Winterwood N, DeMali KA & Stipp CS (2009) Tetraspanin CD151 regulates RhoA activation and the dynamic stability of carcinoma cell-cell contacts. *J Cell Sci* **122**, 2263–2273.
- 30 Charrin S, Jouannet S, Boucheix C & Rubinstein E (2014) Tetraspanins at a glance. *J Cell Sci* **127**, 3641–3648.
- 31 Wright MD & Tomlinson MG (1994) The ins and outs of the transmembrane 4 superfamily. *Immunol Today* **15**, 588–594.
- 32 Zuidsscherwoude M, Gottfert F, Dunlock VM, Figdor CG, van den Bogaart G & van Spriel AB (2015) The tetraspanin web revisited by super-resolution microscopy. *Sci Rep* **5**, 12201.
- 33 Haining EJ, Yang J, Bailey RL, Khan K, Collier R, Tsai S, Watson SP, Frampton J, Garcia P & Tomlinson MG (2012) The TspanC8 subgroup of tetraspanins interacts with A disintegrin and metalloprotease 10 (ADAM10) and regulates its maturation and cell surface expression. *J Biol Chem* **287**, 39753–39765.
- 34 Heikens MJ, Cao TM, Morita C, Dehart SL & Tsai S (2007) Penumbra encodes a novel tetraspanin that is highly expressed in erythroid progenitors and promotes effective erythropoiesis. *Blood* **109**, 3244–3252.
- 35 Luu VP, Hevezi P, Vences-Catalan F, Maravillas-Montero JL, White CA, Casali P, Llorente L, Jakez-Ocampo J, Lima G, Vilches-Cisneros N *et al.* (2013) TSPAN33 is a novel marker of activated and malignant B cells. *Clin Immunol* **149**, 388–399.
- 36 Perez-Martinez CA, Maravillas-Montero JL, Meza-Herrera I, Vences-Catalan F, Zlotnik A & Santos-Argumedo L (2017) Tspan33 is expressed in transitional and memory B cells, but is not responsible for high ADAM10 expression. *Scand J Immunol* **86**, 23–30.
- 37 Ruiz-Garcia A, Lopez-Lopez S, Garcia-Ramirez JJ, Baladron V, Ruiz-Hidalgo MJ, Lopez-Sanz L, Ballesteros A, Laborda J, Monsalve EM & Diaz-Guerra MJ (2016) The tetraspanin TSPAN33 controls TLR-triggered macrophage activation through modulation of NOTCH signaling. *J Immunol* **197**, 3371–3381.
- 38 Dornier E, Coumailleau F, Ottavi JF, Moretti J, Boucheix C, Mauduit P, Schweiguth F & Rubinstein E (2012) TspanC8 tetraspanins regulate ADAM10/Kuzbanian trafficking and promote Notch activation in flies and mammals. *J Cell Biol* **199**, 481–496.
- 39 Dunn CD, Sulis ML, Ferrando AA & Greenwald I (2010) A conserved tetraspanin subfamily promotes Notch signaling in *Caenorhabditis elegans* and in human cells. *Proc Natl Acad Sci USA* **107**, 5907–5912.
- 40 Priyathilaka TT, Bathige S, Herath H, Lee S & Lee J (2017) Molecular identification of disk abalone (*Haliotis discus discus*) tetraspanin 33 and CD63: Insights into potent players in the disk abalone host defense system. *Fish Shellfish Immunol* **69**, 173–184.
- 41 Maravillas-Montero JL, Gillespie PG, Patino-Lopez G, Shaw S & Santos-Argumedo L (2011) Myosin 1c participates in B cell cytoskeleton rearrangements, is recruited to the immunologic synapse, and contributes to antigen presentation. *J Immunol* **187**, 3053–3063.
- 42 Lopez-Ortega O & Santos-Argumedo L (2017) Myosin 1g contributes to CD44 adhesion protein and lipid rafts recycling and controls CD44 capping and cell migration in B lymphocytes. *Front Immunol* **8**, 1731.
- 43 Maravillas-Montero JL, Lopez-Ortega O, Patino-Lopez G & Santos-Argumedo L (2014) Myosin 1g regulates cytoskeleton plasticity, cell migration, exocytosis, and endocytosis in B lymphocytes. *Eur J Immunol* **44**, 877–886.
- 44 Calpe E, Codony C, Baptista MJ, Abrisqueta P, Carpio C, Purroy N, Bosch F & Crespo M (2011) ZAP-70 enhances migration of malignant B lymphocytes toward CCL21 by inducing CCR7 expression via IgM-ERK1/2 activation. *Blood* **118**, 4401–4410.
- 45 Ding N, Ping L, Feng L, Zheng X, Song Y & Zhu J (2014) Histone deacetylase 6 activity is critical for the metastasis of Burkitt's lymphoma cells. *Cancer Cell Int* **14**, 139.
- 46 Lenzo JC, O'Brien-Simpson NM, Cecil J, Holden JA & Reynolds EC (2016) Determination of active phagocytosis of unopsonized *Porphyromonas gingivalis* by macrophages and neutrophils using the pH-sensitive fluorescent dye pHrodo. *Infect Immun* **84**, 1753–1760.
- 47 Overland HS, Pettersen EF, Ronneseth A & Wergeland HI (2010) Phagocytosis by B-cells and neutrophils in Atlantic salmon (*Salmo salar* L.) and Atlantic cod (*Gadus morhua* L.). *Fish Shellfish Immunol* **28**, 193–204.
- 48 Sunyer JO (2012) Evolutionary and functional relationships of B cells from fish and mammals: insights into their novel roles in phagocytosis and presentation of particulate antigen. *Infect Disord Drug Targets* **12**, 200–212.
- 49 Yu M, Yang S, Sun H & Xia Q (2016) CD63 promotes hemocyte-mediated phagocytosis in the clam, *Paphia undulata*. *J Immunol Res* **2016**, 7893490.
- 50 Zhu Q, Zhang M, Shi M, Liu Y, Zhao Q, Wang W, Zhang G, Yang L, Zhi J, Zhang L *et al.* (2016) Human B cells have an active phagocytic capability and undergo immune activation upon phagocytosis of

- Mycobacterium tuberculosis*. *Immunobiology* **221**, 558–567.
- 51 Zimmerman LM, Vogel LA, Edwards KA & Bowden RM (2010) Phagocytic B cells in a reptile. *Biol Lett* **6**, 270–273.
- 52 Chang CH, Lee HH & Lee CH (2017) Substrate properties modulate cell membrane roughness by way of actin filaments. *Sci Rep* **7**, 9068.
- 53 Lopez-Ortega O, Ovalle-Garcia E, Ortega-Blake I, Antillon A, Chavez-Munguia B, Patino-Lopez G, Fragoso-Soriano R & Santos-Argumedo L (2016) Myo1g is an active player in maintaining cell stiffness in B-lymphocytes. *Cytoskeleton* **73**, 258–268.
- 54 Ovalle-Garcia E, Torres-Heredia JJ, Antillon A & Ortega-Blake I (2011) Simultaneous determination of the elastic properties of the lipid bilayer by atomic force microscopy: bending, tension, and adhesion. *J Phys Chem B* **115**, 4826–4833.
- 55 Sala-Valdes M, Ursua A, Charrin S, Rubinstein E, Hemler ME, Sanchez-Madrid F & Yanez-Mo M (2006) EWI-2 and EWI-F link the tetraspanin web to the actin cytoskeleton through their direct association with ezrin-radixin-moesin proteins. *J Biol Chem* **281**, 19665–19675.
- 56 van Deventer SJ, Dunlock VE & van Spriel AB (2017) Molecular interactions shaping the tetraspanin web. *Biochem Soc Trans* **45**, 741–750.
- 57 Gartlan KH, Wee JL, Demaria MC, Nastovska R, Chang TM, Jones EL, Apostolopoulos V, Pietersz GA, Hickey MJ, van Spriel AB *et al.* (2013) Tetraspanin CD37 contributes to the initiation of cellular immunity by promoting dendritic cell migration. *Eur J Immunol* **43**, 1208–1219.
- 58 Reyes R, Monjas A, Yanez-Mo M, Cardenes B, Morlino G, Gilsanz A, Machado-Pineda Y, Lafuente E, Monk P, Sanchez-Madrid F *et al.* (2015) Different states of integrin LFA-1 aggregation are controlled through its association with tetraspanin CD9. *Biochim Biophys Acta* **1853**, 2464–2480.
- 59 Osvaldova A, Stepanova H, Faldyna M & Matiasovic J (2017) Gene expression values of pattern-recognition receptors in porcine leukocytes and their response to *Salmonella enterica* serovar Typhimurium infection. *Res Vet Sci* **114**, 31–35.
- 60 Jouannet S, Saint-Pol J, Fernandez L, Nguyen V, Charrin S, Boucheix C, Brou C, Milhiet PE & Rubinstein E (2016) TspanC8 tetraspanins differentially regulate the cleavage of ADAM10 substrates, Notch activation and ADAM10 membrane compartmentalization. *Cell Mol Life Sci* **73**, 1895–1915.
- 61 Saint-Pol J, Eschenbrenner E, Dornier E, Boucheix C, Charrin S & Rubinstein E (2017) Regulation of the trafficking and the function of the metalloprotease ADAM10 by tetraspanins. *Biochem Soc Trans* **45**, 937–944.
- 62 Huttlin EL, Bruckner RJ, Paulo JA, Cannon JR, Ting L, Baltier K, Colby G, Gebreab F, Gygi MP, Parzen H *et al.* (2017) Architecture of the human interactome defines protein communities and disease networks. *Nature* **545**, 505–509.
- 63 Stark C, Breitkreutz BJ, Reguly T, Boucher L, Breitkreutz A & Tyers M (2006) BioGRID: a general repository for interaction datasets. *Nucleic Acids Res* **34**, D535–D539.
- 64 Bari R, Guo Q, Xia B, Zhang YH, Giesert EE, Levy S, Zheng JJ & Zhang XA (2011) Tetraspanins regulate the protrusive activities of cell membrane. *Biochem Biophys Res Commun* **415**, 619–626.
- 65 McConnell RE, Higginbotham JN, Shifrin DA Jr, Tabb DL, Coffey RJ & Tyska MJ (2009) The enterocyte microvillus is a vesicle-generating organelle. *J Cell Biol* **185**, 1285–1298.
- 66 Israels SJ & McMillan-Ward EM (2007) Platelet tetraspanin complexes and their association with lipid rafts. *Thromb Haemost* **98**, 1081–1087.
- 67 Runge KE, Evans JE, He ZY, Gupta S, McDonald KL, Stahlberg H, Primakoff P & Myles DG (2007) Oocyte CD9 is enriched on the microvillar membrane and required for normal microvillar shape and distribution. *Dev Biol* **304**, 317–325.
- 68 Inoue S, Kondo S, Parchy DM & Watanabe M (2014) Tetraspanin 3c requirement for pigment cell interactions and boundary formation in zebrafish adult pigment stripes. *Pigment Cell Melanoma Res* **27**, 190–200.
- 69 Greicius G, Westerberg L, Davey EJ, Buentke E, Scheynius A, Thyberg J & Severinson E (2004) Microvilli structures on B lymphocytes: inducible functional domains? *Int Immunol* **16**, 353–364.
- 70 Lee J, Byun HJ, Lee MS, Jin YJ, Jeoung D, Kim YM & Lee H (2017) The metastasis suppressor CD82/KAI1 inhibits fibronectin adhesion-induced epithelial-to-mesenchymal transition in prostate cancer cells by repressing the associated integrin signaling. *Oncotarget* **8**, 1641–1654.
- 71 Delaguillaumie A, Lagaudriere-Gesbert C, Popoff MR & Conjeaud H (2002) Rho GTPases link cytoskeletal rearrangements and activation processes induced via the tetraspanin CD82 in T lymphocytes. *J Cell Sci* **115**, 433–443.
- 72 Martinez del Hoyo G, Ramirez-Huesca M, Levy S, Boucheix C, Rubinstein E, Minguito de la Escalera M, Gonzalez-Cintado L, Ardavin C, Veiga E, Yanez-Mo M *et al.* (2015) CD81 controls immunity to *Listeria* infection through rac-dependent inhibition of proinflammatory mediator release and activation of cytotoxic T cells. *J Immunol* **194**, 6090–6101.

- 73 Rocha-Perugini V, Martinez Del Hoyo G, Gonzalez-Granado JM, Ramirez-Huesca M, Zorita V, Rubinstein E, Boucheix C & Sanchez-Madrid F (2017) CD9 regulates major histocompatibility complex class II trafficking in monocyte-derived dendritic cells. *Mol Cell Biol* **37**, 1–17.
- 74 Lebakken CS, McQuade KJ & Rapraeger AC (2000) Syndecan-1 signals independently of beta1 integrins during Raji cell spreading. *Exp Cell Res* **259**, 315–325.
- 75 Shaw AR, Domanska A, Mak A, Gilchrist A, Dobler K, Visser L, Poppema S, Fliegel L, Letarte M & Willett BJ (1995) Ectopic expression of human and feline CD9 in a human B cell line confers beta 1 integrin-dependent motility on fibronectin and laminin substrates and enhanced tyrosine phosphorylation. *J Biol Chem* **270**, 24092–24099.
- 76 Wee JL, Schulze KE, Jones EL, Yeung L, Cheng Q, Pereira CF, Costin A, Ramm G, van Spriel AB, Hickey MJ *et al.* (2015) Tetraspanin CD37 regulates beta2 integrin-mediated adhesion and migration in neutrophils. *J Immunol* **195**, 5770–5779.
- 77 Diz-Munoz A, Thurley K, Chintameni S, Altschuler SJ, Wu LF, Fletcher DA & Weiner OD (2016) Membrane tension acts through PLD2 and mTORC2 to limit actin network assembly during neutrophil migration. *PLoS Biol* **14**, e1002474.
- 78 Bennett M, Cantini M, Reboud J, Cooper JM, Roca-Cusachs P & Salmeron-Sanchez M (2018) Molecular clutch drives cell response to surface viscosity. *Proc Natl Acad Sci USA* **115**, 1192–1197.
- 79 Elosegui-Artola A, Oriá R, Chen Y, Kosmalska A, Perez-Gonzalez C, Castro N, Zhu C, Trepaut X & Roca-Cusachs P (2016) Mechanical regulation of a molecular clutch defines force transmission and transduction in response to matrix rigidity. *Nat Cell Biol* **18**, 540–548.
- 80 Pontes B, Monzo P & Gauthier NC (2017) Membrane tension: a challenging but universal physical parameter in cell biology. *Semin Cell Dev Biol* **71**, 30–41.
- 81 Murphy DA & Courtneidge SA (2011) The 'ins' and 'outs' of podosomes and invadopodia: characteristics, formation and function. *Nat Rev Mol Cell Biol* **12**, 413–426.
- 82 Berditchevski F & Odintsova E (2007) Tetraspanins as regulators of protein trafficking. *Traffic* **8**, 89–96.
- 83 Andreu Z & Yanez-Mo M (2014) Tetraspanins in extracellular vesicle formation and function. *Front Immunol* **5**, 442.
- 84 Mazurov D, Barbashova L & Filatov A (2013) Tetraspanin protein CD9 interacts with metalloprotease CD10 and enhances its release via exosomes. *FEBS J* **280**, 1200–1213.
- 85 Sens P & Turner MS (2006) Budded membrane microdomains as tension regulators. *Phys Rev Stat Nonlin Soft Matter Phys* **73**, 031918.
- 86 Li J, Barreda DR, Zhang YA, Boshra H, Gelman AE, Lapatra S, Tort L & Sunyer JO (2006) B lymphocytes from early vertebrates have potent phagocytic and microbicidal abilities. *Nat Immunol* **7**, 1116–1124.
- 87 LaFoya B, Munroe JA, Miyamoto A, Detweiler MA, Crow JJ, Gazdik T & Albig AR (2018) Beyond the matrix: the many non-ECM ligands for integrins. *Int J Mol Sci* **19**, 1–33.
- 88 Dupuy AG & Caron E (2008) Integrin-dependent phagocytosis: spreading from microadhesion to new concepts. *J Cell Sci* **121**, 1773–1783.
- 89 Pontes B, Ayala Y, Fonseca AC, Romao LF, Amaral RF, Salgado LT, Lima FR, Farina M, Viana NB, Moura-Neto V *et al.* (2013) Membrane elastic properties and cell function. *PLoS ONE* **8**, e67708.
- 90 Simunovic M, Bassereau P & Voth GA (2018) Organizing membrane-curving proteins: the emerging dynamical picture. *Curr Opin Struct Biol* **51**, 99–105.
- 91 Keren K (2011) Cell motility: the integrating role of the plasma membrane. *Eur Biophys J* **40**, 1013–1027.
- 92 Raucher D & Sheetz MP (2000) Cell spreading and lamellipodial extension rate is regulated by membrane tension. *J Cell Biol* **148**, 127–136.
- 93 Gauthier NC, Masters TA & Sheetz MP (2012) Mechanical feedback between membrane tension and dynamics. *Trends Cell Biol* **22**, 527–535.
- 94 Liu Y, Belkina NV, Park C, Nambiar R, Loughhead SM, Patino-Lopez G, Ben-Aissa K, Hao JJ, Kruhlak MJ, Qi H *et al.* (2012) Constitutively active ezrin increases membrane tension, slows migration, and impedes endothelial transmigration of lymphocytes *in vivo* in mice. *Blood* **119**, 445–453.
- 95 Rouven Bruckner B, Pietuch A, Nehls S, Rother J & Janshoff A (2015) Ezrin is a major regulator of membrane tension in epithelial cells. *Sci Rep* **5**, 14700.
- 96 Barnhart EL, Lee KC, Keren K, Mogilner A & Theriot JA (2011) An adhesion-dependent switch between mechanisms that determine motile cell shape. *PLoS Biol* **9**, e1001059.
- 97 Gerard A, Patino-Lopez G, Beemiller P, Nambiar R, Ben-Aissa K, Liu Y, Totah FJ, Tyska MJ, Shaw S & Krummel MF (2014) Detection of rare antigen-presenting cells through T cell-intrinsic meandering motility, mediated by Myo1g. *Cell* **158**, 492–505.
- 98 Girasole M, Pompeo G, Cricenti A, Congiu-Castellano A, Andreola F, Serafino A, Frazer BH, Boumis G & Amiconi G (2007) Roughness of the plasma membrane as an independent morphological parameter to study RBCs: a quantitative atomic force microscopy investigation. *Biochim Biophys Acta* **1768**, 1268–1276.
- 99 Wang Y, Xu C, Jiang N, Zheng L, Zeng J, Qiu C, Yang H & Xie S (2016) Quantitative analysis of the cell-surface roughness and viscoelasticity for breast cancer cells discrimination using atomic force microscopy. *Scanning* **38**, 558–563.

- 100 Ono M, Handa K, Sonnino S, Withers DA, Nagai H & Hakomori S (2001) GM3 ganglioside inhibits CD9-facilitated haptotactic cell motility: coexpression of GM3 and CD9 is essential in the downregulation of tumor cell motility and malignancy. *Biochemistry* **40**, 6414–6421.
- 101 Odintsova E, Voortman J, Gilbert E & Berditchevski F (2003) Tetraspanin CD82 regulates compartmentalisation and ligand-induced dimerization of EGFR. *J Cell Sci* **116**, 4557–4566.
- 102 Page K & Lange Y (1997) Cell adhesion to fibronectin regulates membrane lipid biosynthesis through 5'-AMP-activated protein kinase. *J Biol Chem* **272**, 19339–19342.
- 103 Roduit C, van der Goot FG, De Los Rios P, Yersin A, Steiner P, Dietler G, Catsicas S, Lafont F & Kasas S (2008) Elastic membrane heterogeneity of living cells revealed by stiff nanoscale membrane domains. *Biophys J* **94**, 1521–132.
- 104 Hao JJ, Wang G, Pisitkun T, Patino-Lopez G, Nagashima K, Knepper MA, Shen RF & Shaw S (2008) Enrichment of distinct microfilament-associated and GTP-binding-proteins in membrane/microvilli fractions from lymphoid cells. *J Proteome Res* **7**, 2911–2927.
- 105 Haeussler M, Schonig K, Eckert H, Eschstruth A, Mianne J, Renaud JB, Schneider-Maunoury S, Shkumatava A, Teboul L, Kent J *et al.* (2016) Evaluation of off-target and on-target scoring algorithms and integration into the guide RNA selection tool CRISPOR. *Genome Biol* **17**, 148.
- 106 Bauer DE, Canver MC & Orkin SH (2015) Generation of genomic deletions in mammalian cell lines via CRISPR/Cas9. *J Vis Exp* **95**, e52118.